Marine and Petroleum Geology 112 (2020) 104063

Contents lists available at ScienceDirect

Marine and Petroleum Geology

journal homepage: www.elsevier.com/locate/marpetgeo

Research paper

Influence of multistage oil emplacement on carbonate cementation in the Eocene Shahejie Formation, Dongying Sag, Bohai Bay Basin, China

Wang Yanzhong[a,*], Xie Qiangwang[a], Cao Yingchang[a], Lin Miruo[a], Wang Yongshi[b], Li Yuzhi[c], Wang Xin[c], Xi Kelai[a], Mi Lianshan[d], Guo Yingchun[e], Du yujie[a]

[a] School of Geosciences, China University of Petroleum, Qingdao, Shandong, 266580, China
[b] Shengli Oilfield, SINOPEC, Dongying, Shandong, 257015, China
[c] Dongxin Oil Production Plant, Shengli Oilfield, SINOPEC, Dongying, Shandong, 257061, China
[d] Shengli Oil Production Plant, Shengli Oilfield, SINOPEC, Dongying, Shandong, 257000, China
[e] Exploration and Development Research Institute, Shengli Oilfield, SINOPEC, Dongying, Shandong, 257000, China

ARTICLE INFO

Keywords:
Carbonate cementation
Multistage oil emplacement
Sequence of oil emplacement and carbonate cementation
Dongying sag

ABSTRACT

The influence of multi-stage oil emplacement on carbonate cementation was investigated on the basis of determining the sequence of oil emplacement and carbonate cementation in the clastic reservoirs of the upper part of the fourth member of the Eocene Shahejie Formation (Es4s) in the Yanxie 229 area, Dongying Sag. The sequence of multistage oil emplacement and carbonate cementation was determined by projecting the homogenization temperatures (Ths) of two-phase aqueous inclusions on a burial and thermal history plot. The ratio of the number of quartz grains with yellow-fluorescent oil inclusions therein to the total number of quartz grains (YGOI) and the ratio of the number of quartz grains with blue-fluorescent oil inclusions therein to the total number of quartz grains (BGOI) were calculated to analyze the paleo-oil saturation of each stage of oil emplacement. The YGOI and BGOI values reflect the relative level of the paleo-oil saturation of the first-stage yellow-fluorescent (FSYF) oil and the second-stage blue-fluorescent (SSBF) oil, respectively. A large number of primary pores were preserved in the oil layers, whereas only a small number of dissolution pores and micropores were developed in the oil-bearing water layers and dry layers. Calcite, dolomite, ferrocalcite, and ankerite cementation and two-stage oil emplacement occurred in the Es4s reservoirs. The FSYF oil emplacement occurred earlier than the ankerite cementation and ferrocalcite cementation but later than the calcite cementation and dolomite cementation. The SSBF oil emplacement occurred later than all phases of carbonate cementation. The dolomite cementation was not influenced by the FSYF oil emplacement because it occurred earlier than the FSYF oil emplacement. The ankerite cementation was dominantly inhibited by the FSYF oil emplacement in the oil layers and the degree of inhibition increased with the increase in paleo-oil saturation of the FSYF oil. The SSBF oil emplacement further increased the paleo-oil saturation in the oil layers, which enhanced the inhibition of the ankerite cementation and even stopped it. The ankerite cementation in the dry layers and oil-bearing water layers was slowed down or stopped due to the lack of pores and the low transportation rate of external material, which was caused by the intense ankerite cementation prior to the SSBF oil emplacement.

1. Introduction

The origin and distribution of high-quality clastic reservoirs are the keys to petroleum exploration. Diagenesis is a significant factor influencing reservoir quality (Gluyas et al., 1993; Gaupp et al., 1993; Dutton and Loucks, 2010; Taylor et al., 2010; Bjørlykke. et al., 2012; Xi et al., 2015a; Ma et al., 2016; Yuan et al., 2018). Much attention has been focused on the factors influencing diagenesis (Mansurbeg et al., 2008; Xi et al., 2015a; Ma et al., 2016). Oil emplacement is considered an important factor influencing cementation in clastic reservoirs (Saigal et al., 1992; Wang et al., 1998; Bloch et al., 2002; Friis et al., 2014; Worden et al., 2018; Yuan et al., 2019). However, the influence of oil emplacement on cementation is still a controversial topic. Some scholars argued that oil emplacement can inhibit cementation and preserve porosity (Walderhaug, 1990; Saigal et al., 1992; Oxtoby et al., 1995; Worden et al., 1998, 2018; Cai et al., 2001; Molenaar et al., 2008; Taylor et al., 2010; Neveux et al., 2014; Kolchugin et al., 2016; Paganni et al., 2016). This view point is based on the differences in porosity and

* Corresponding author.
E-mail address: wangyanzhong1980@163.com (W. Yanzhong).

https://doi.org/10.1016/j.marpetgeo.2019.104063
Received 20 March 2019; Received in revised form 1 September 2019; Accepted 25 September 2019
Available online 27 September 2019
0264-8172/

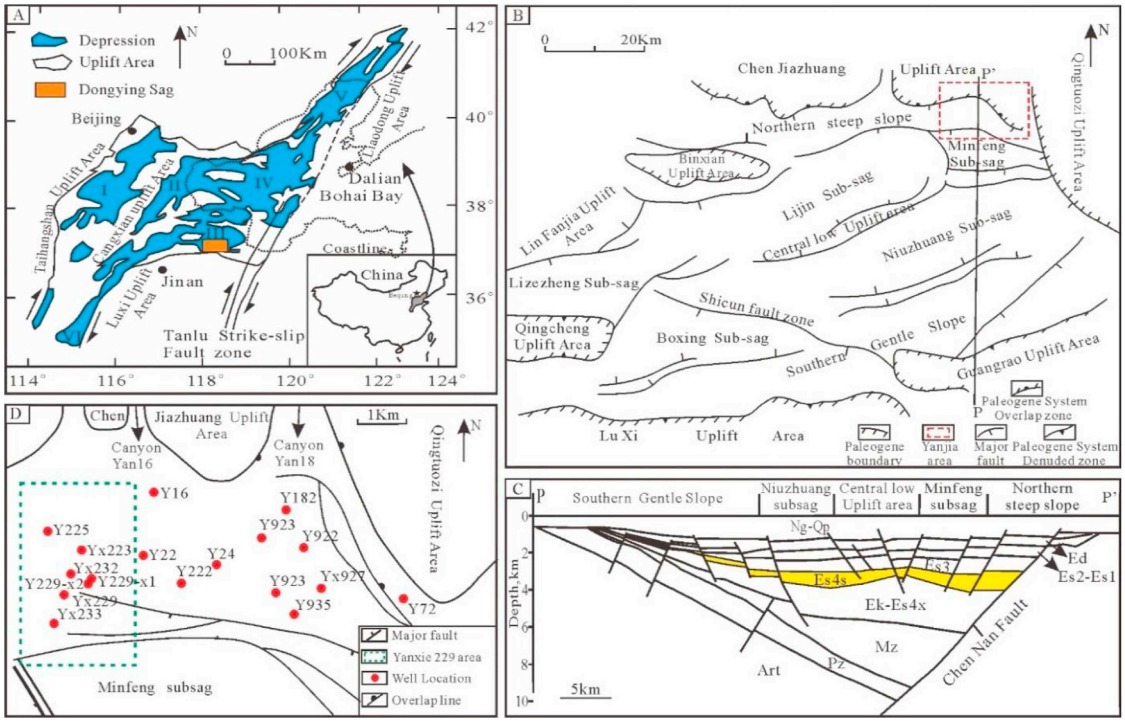

Fig. 1. (A) Location map of the Dongying Sag in the Jiyang Sub-basin (III) of the Bohai Bay Basin. Other Sub-basins in the Bohai Bay Basin in Eastern China include the Jizhong Sub-basin (I), Huanghua Sub-basin (II), Bozhong Sub-basin (IV), Liaohe Sub-basin (V), and Dongpu Sub-basin (VI) (Yang et al., 2017). The black rectangle filled with orange colour shows the location of the Dongying Sag. (B) Structural map of the Dongying Sag showing the distribution of the main Sub-sags, uplift areas, and major faults and the location of P–P'. (C) South-to-north cross-section P–P′ showing the major stratigraphic units and major tectonic features within the Dongying Sag. Q: Quaternary Period; Nm: Neocene Minghuazhen Formation; Ng: Neocene Guantao Formation; Ed: Paleogene Dongying Formation; Es1: The first member of the Paleogene Shahejie Formation (Es); Es2: The second member of Es; Es3 The third member of Es; Es4: The fourth member of Es; Es4s: the upper part of the Es4; Es4x: the lower part of the Es4; Ek: Paleogene Kongdian Formation. (D) Map showing the location of the study area and well locations in the Yanjia area. The red dashed box in Fig. 1B is the location of the Yanjia area. The green dashed box is the location of the study area called the Yanxie229 area. (For interpretation of the references to color in this figure legend, the reader is referred to the Web version of this article.)

permeability, the cement content, the characteristics of the inclusions and the isotope ratio difference between the oil and water zones (Prozorovich, 1970; Hawkins, 1978; Dixon et al., 1989; Marchand et al., 2000, 2001; Paganoni et al., 2015; Worden et al., 2018). Researchers have proposed that (1) the relative permeability of the water phase is very low in externally-sourced, water-wet/oil-wet clastic reservoirs under the condition of high oil saturation, leading to the inhibition of cementation (Walderhaug, 1990; Saigal et al., 1992; Worden et al., 1998; Worden and Morad, 2000; Cai et al., 2001; Molenaar et al., 2008; Taylor et al., 2010; Neveux et al., 2014; Kolchugin et al., 2016; Paganni et al., 2016; Ehrenberg et al., 2016), (2) the diffusion rate is so low that the cementation is basically stopped because the diffusion paths are more tortuous under the condition of high oil saturation in internally-sourced water-wet clastic reservoirs (Walderhaug, 1990; Worden et al., 1998; Sathar et al., 2012; Bukar, 2013; Friis et al., 2014), and (3) the oil films on the surfaces of grains inhibit pressure dissolution and material supply and prevent the pore water from contacting the grains in internally-sourced oil-wet clastic reservoirs, resulting in the inhibition of cementation (Worden et al., 1998; Neilson et al., 1998; Bukar, 2013; Neveux et al., 2014). In contrast, other scholars have argued that cementation is largely unhindered by oil emplacement. They proposed that the diffusion of materials would be continued in water films on mineral surfaces or in residual water under the condition of maximum oil saturation and that cementation would not be inhibited in clastic reservoirs (Bjørkum and Walderhaug, 1993; Nedkvitne et al., 1993; Barclay and Worden, 2000; Worden and Morad, 2000; Bloch et al., 2002; Aase and Walderhaug, 2005; Taylor et al., 2010; Yuan et al., 2011). Consequently, the porosity, permeability, cement content, and isotopic characteristics between oil and water layers exhibit few differences (Ehrenberg, 1990; Giles et al., 1992; Ramm and Bjørlykke, 1994; Aase and Walderhaug, 2005; Molenaar et al., 2008).

In the process of researching the influence of oil emplacement on cementation, the sequence of oil emplacement and cementation needs to be seriously considered (Worden and Morad, 2000; Bloch et al., 2002; Worden et al., 2018). For example, if oil was emplaced following cementation, there is no reason why oil and water layers in the reservoirs should have different quantities of cement (Worden and Morad, 2000; Bloch et al., 2002). However, the sequence of oil emplacement and cementation was not clearly defined in some statistical analyses (Haszeldine et al., 2003; Cai et al., 2001). It is not appropriate to discuss the influence of oil emplacement on cementation without defining the sequence of oil emplacement and cementation (Marchand et al., 2002; Worden et al., 2018).

Oil saturation may influence the internal sourcing rates and transport rate in the reservoirs and then significantly affect the subsequent diagenesis (Worden et al., 1998). The present oil saturation was used to analyze the influence of oil emplacement on cementation (Gong et al., 2016; Worden et al., 2018). However the present oil saturation is the sum of the individual charge episodes in the reservoirs with multistage oil emplacement (Marchand et al., 2002; Tobin et al., 2010; Paganoni et al., 2015; Worden et al., 2018). It is essential to introduce the paleo-oil saturation of each stage of the oil emplacement. However, the influence of the paleo-oil saturation of each stage of the oil emplacement on cementation has been rarely investigated in reservoirs with a complex sequence of multistage hydrocarbon emplacement and cementation (Cox et al., 2010; Paganoni et al., 2015).

Current research has mostly focused on the influence of oil emplacement on the cementation of quartz and clay minerals (Prozorovich, 1970; Hamilton et al., 1992; Bjørkum and Walderhaug, 1993; Marchand et al., 2001; Taylor et al., 2010; Worden et al., 2018). The

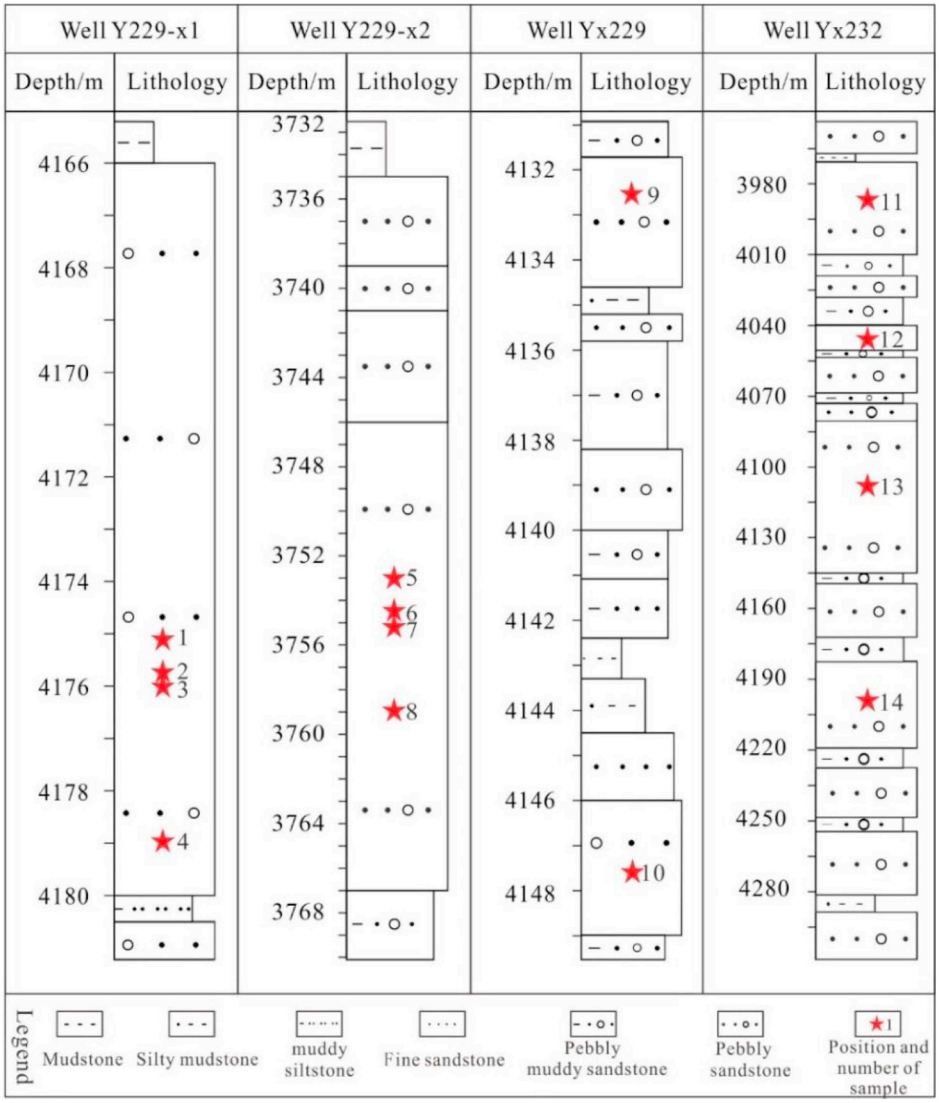

Fig. 2. Lithologic columns showing the lithology and the positions of the samples. The location of the wells Y229-x1, Y229-x2, Yx229, and Yx232 is shown in Fig. 1D. The lithology of the wells Y229-x1 and Y229-x2 was described based on the core. The lithology of the wells Yx229 and Yx232 was described based on the drilling cuttings. The red five-pointed stars numbered 1–14 represent the positions of the typical samples. All the typical samples are pebbly sandstones. Samples 1–4 are from dry layers, samples 5–10 are from oil layers, and samples 11–14 are from oil-bearing water layers. (For interpretation of the references to color in this figure legend, the reader is referred to the Web version of this article.)

influence of the oil emplacement on the carbonate cementation in clastic reservoirs was rarely discussed (Kolchugin et al., 2016; Paganni et al., 2016). Simple comparisons of the carbonate cement content between the oil and water layers in clastic reservoirs were conducted by some researchers (Cox et al., 2010; Bukar, 2013; Neveux, 2014; JI et al., 2015). However, carbonate cementation has also a significant influence on reservoir quality in clastic reservoirs (Morad et al., 2012; Wang et al., 2014; Cao et al., 2016; Yang et al., 2017). Therefore, the objective of this study is to discuss the influence of multistage oil emplacement on carbonate cementation in clastic reservoirs by establishing the sequence of oil emplacement and carbonate cementation and excluding influencing factors other than oil emplacement.

2. Geological background

The Dongying Sag is located in the south-eastern part of the Jiyang Sub-basin of the Bohai Bay Basin in Eastern China (Fig. 1A). It is a Mesozoic-Cenozoic half graben rift-down warped basin with lacustrine deposits directly deposited on Paleozoic bedrocks (Cao et al., 2014; Wang et al., 2014). The Dongying Sag is bounded to the east by the Qingtuozi uplift area, to the south by the Luxi and Guangrao uplift areas, to the west by the Linfanjia and Gaoqing uplift areas, and to the north by the Chenjiazhuang-Binxian uplift area (Fig. 1B). It covers an area of 5850 km^2 with an east-west and north-south extent of 90 km and 65 km, respectively. In cross-section, it is a half graben with a fault-controlled northern steep margin and a southern gentle margin (Fig. 1C). In planar view, the Dongying Sag is further subdivided into several secondary structural units, such as the northern steep slope zone, the central low uplift area, the Lijin, Minfeng, Niuzhuang and Boxing Sub-sags, and the southern gentle slope zone (Zhang et al., 2014, Fig. 1B). The Paleogene in the Dongying Sag can be divided from bottom to top into the Kongdian, Shahejie, and Dongying Formations. The Shahejie Formation can be further subdivided from bottom to top into the Fourth Member (Es4), the Third Member (Es3), the Second Member (Es2) and the First Member (Es1), respectively. The Es4 consists of the upper part (Es4s) and the lower part (Es4x) (Wang et al., 2014, 2016; Cao et al., 2018).

The Yanjia area is located in the northern part of the Minfeng Sub-sag, which lies in the north-eastern part of the Dongying Sag (Fig. 1B). The Yanjia area is a steep slope zone controlled by the Chennan listric normal fault where two canyons named Yan 16 and Yan 18 were developed (Cao et al., 2018, Fig. 1C and D). The Yanxie229 area is located in the western part of the Yanjia area, where the canyon of Yan16 was developed (Cao et al., 2018, Fig. 1D). The canyon of Yan16 was the source feeder channels of debris flows. During the accumulation of the Es4s, terrigenous sediments were transported into the deep water along the canyons of Yan16. The mountain-derived floods and normal mountain-derived river discharges and were accumulated on the

downthrown side of the Chennan fault in the Yanxie229 area, forming large-scale sandstones and conglomerates of nearshore subaqueous fans close to deep-water source rocks (Cao et al., 2018). The pebbly sandstones in the Es4s in the Yanxie229 area are the predominant research object of this study. There is a complex alternating relationship between multi-stage hydrocarbon emplacement and carbonate cementation in the northern steep slope zone of the Minfeng Sub-sag. (Wang et al., 2014, 2016).

3. Samples and methodology

3.1. Samples

A total of 8 core samples were obtained from wells Y229-x1 and Y229-x2 and 49 side well coring samples were obtained from wells Yx229, Yx232, and Yx233. All samples were taken from the middle fans of the near-shore subaqueous fans in the Es4s in the Yanxie229 area. The positions of the 8 core samples of the pebbly sandstones and the 6 typical side well coring samples of the pebbly sandstones are far away from the sandstone and mudstone interface (Fig. 2). The oiliness of the samples was interpreted by the Exploration and Development Research Institution of the Sinopec Shengli Oil field using well-logging data. Based on the interpreted oil saturation, the oil-bearing grade of the reservoirs is divided into an oil layer, water-bearing oil layer, oil-bearing water layer, and water layer. The oil saturations in the oil layers, water-bearing oil layers, oil-bearing water layers, and water layers are above 50%, 30%–50%, 10–30%, and below 10%, respectively. Dry layers are defined as reservoirs with a daily fluid production lower than the specified yield standard of fluid, which is determined by burial depth and fluid types . The interpretation results show that 6 samples are from oil layers, 4 samples are from oil-bearing water layers, and 4 samples are from dry layers (Fig. 2).

3.2. Methodology

A total of 57 blue epoxy resin-impregnated thin sections partly stained with Alizarin Red S and K-ferricyanide were prepared for observation of the rock mineralogy, diagenesis, and the pores. These thin-sections were observed under a Zeiss Axio Lab.A1 Pol optical microscope. The thin-section contents of the framework grains, matrices, and authigenic cements were determined using the following method. First, 5 typical view fields in each thin-section were chosen and photomicrographs were obtained using a 10 × objective but higher power objectives were used where necessary. Second, the thin-section areas of the different types of framework grains, matrices, and cements in each photomicrograph were sketched and calculations were performed using the Axio Vision software Rel. Finally, the thin-section contents of the different types of framework grains, matrices, and cements were determined by averaging the values of the 5 view fields in each thin section. Scanning electron microscope (SEM) images were acquired using a Quanta200 scanning electron microscope combined with energy-dispersive X-ray spectroscopy. Cathodoluminescence (CL) analysis and electron microprobe point analysis (EMPA) were conducted to distinguish the different carbonate cements. The CL analyses of 27 typical samples were conducted under a Zeiss Axio Lab.A1 Pol optical microscope equipped with a CL8200-MKSCL instrument at an accelerating voltage of 15 kV.

The EPMA was conducted using a JEOLJXA-8230 microanalyzer equipped with a 3-channel spectrometer and energy dispersive spectrometer (EDS) (INCAx-act350) at the Ocean University of China. The microanalyzer has an acceleration voltage of 20 kV, an electric current of 1×10^{-8} A, and a spot size of 5–10 μm. Element test range: B ~ U. The chemical analysis values yielded by EPMA were accurate to within about 1 wt% for the major elements and 3 wt% for the trace elements. The element analysis was calibrated using natural and synthetic standards and the following materials: MgO-diopside, CaO-diopside, FeO-hematite, and MnO-bustamite. Limits of detection (three sigma) were 213 ppm for Sr, 116 ppm for Mg, 114 ppm for K, 154 ppm for Ca, 227 ppm for Ti, 199 ppm for Fe, 200 ppm for Cr, and 207 ppm for Mn.

A total of fourteen fluorescence thin sections were prepared for fluorescence observation. The fluorescence thin sections were not heated and soaked nor cleaned with any organic solvent during the preparation. In addition, alpha-cyanoacrylate glue was used to attach the thin sections. Fluorescence was observed using a ZEISS ImagerA1 equipped with ultraviolet (UV) epi-illumination.

Twelve samples were prepared as thick doubly polished thin sections for petrographic analysis, fluorescent color observation, and homogenization temperature measurement of the fluid inclusions.

The observation of petrographic characteristics was conducted using a Zeiss Scope A1 optical microscope-equipped UV light. Useable oculars were 10X with a 1.25X or 1.6X magnification changer. Useable magnification of objectives were 10X, 50X, and 100X. Fluid inclusion assemblages (FIA) were determined according to the position of fluid inclusions in the host minerals. The fluid inclusions without any signs of stretching or partial leakage were used to measure the homogenization temperatures (Ths). The microthermometry of the vapor-liquid two-phase aqueous inclusions was conducted using a Zeiss Scope A1 optical microscope equipped with a calibrated Linkam THMSG 600 heating-cooling stage. The phase transitions can be recorded in the temperature range from −180 °C to 500 °C. The heating rates were 10 °C/min at temperatures below 80 °C and 5 °C/min at temperatures higher than 80 °C. The manufacturer's stated accuracy for the calibration standards (synthetic reference inclusions) is better than 1 °C in the range of temperatures reported here.

We used the method of calculating the grain-containing oil inclusion (GOI) values (Eadington et al., 1996) to determine the ratio of the number of quartz grains with yellow-fluorescent oil inclusions therein to the total number of quartz grains (YGOI) and the ratio of the number of quartz grains with blue-fluorescent oil inclusions therein to the total number of quartz grains (BGOI) of the 6 oil-layer samples, 4 oil-bearing water layer samples, and 4 dry layer samples. The following factors were considered during the calculation of the YGOI and BGOI. (1) Only the oil inclusions in the quartz grains were counted considering the wettability and contents of the grains. (2) More than 200 quartz grains were counted in each sample to minimize the error. (3) The stretched or leaked oil inclusions and the oil inclusions which contained bitumen adhering to the inclusion walls were all excluded because the fluorescence of these types of oil inclusions might have changed (Stasiuk and Snowdon, 1997; Munz, 2001). (4) The blue- and yellow-fluorescent oil inclusions in the quartz grains were counted separately to calculate the BGOI and YGOI.

The Ths of the vapor-liquid two-phase aqueous inclusions coeval with the oil inclusions were projected on the burial and thermal history plot of the corresponding well to determine the periods of hydrocarbon emplacement. The Ths of the vapor-liquid two-phase aqueous inclusions in the carbonate cements were projected on the burial and thermal history plot of the corresponding well to determine the precipitation periods of the carbonate cements. The sequence of oil emplacement and carbonate cementation can be determined based on these periods.

The burial and thermal histories of the wells Yx229, Yx232, Y229-x1, Y229-x2, and Y22-22 were recovered using the 1-D Basin Mod software. The data of lithology mixes, depositional age, and eroded thicknesses of formations and events and other geochemical parameters such as the bottom-hole temperature (BHT) and paleo-geothermal gradient were used to model the burial-thermal history. Absolute ages of depositional and erosional events were defined using the chronostratigraphic framework of the basin (Guo et al., 2012). The initial porosity and compaction factor of a pure lithology (e.g. shale/mudstone, sandstone, siltstone, limestone, and dolomite) were used a default values in the BasinMod 1D software. The missing thickness (the erosion thickness) was obtained from Wu and Han (2000) and Bian

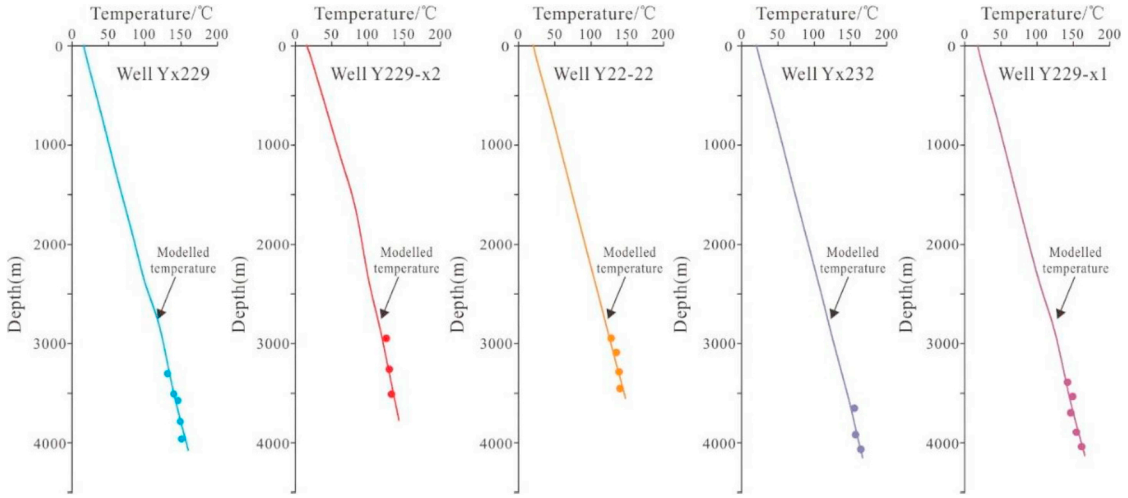

Fig. 3. Calibration of thermal modeling for the wells Y22-22, Yx229, Yx232, Y229-x2, and Y229-x2, showing good correlations between the measured temperatures (solid circles) and modeled temperatures (solid lines).

(2009). Mixed lithologies were created by specifying percentages of the pure lithologies for one-dimensional modeling of individual wells. The cutting logging data and core samples were collected from the Shengli Oilfield, SINOPEC. The thermal history model was obtained in the BasinMod 1D software using the geothermal gradient data obtained by Qiu et al. (2006). The BHT was used to calibrate the thermal history model (Fig. 3). Good correlations between the measured and calculated temperatures were observed (Fig. 3).

4. Results

4.1. Lithology

The reservoirs of the Es4s in the Yanxie229 area are predominantly composed of pebbly sandstones and sandstones which are dominated by lithic feldsarenites and feldspathic litharenites based on the thin section analysis (Fig. 4, Table 1). The pebbly sandstones are poorly sorted with angular or sub-angular grains. The sandstones are moderately sorted with sub-angular or sub-rounded grains. The compositional maturity

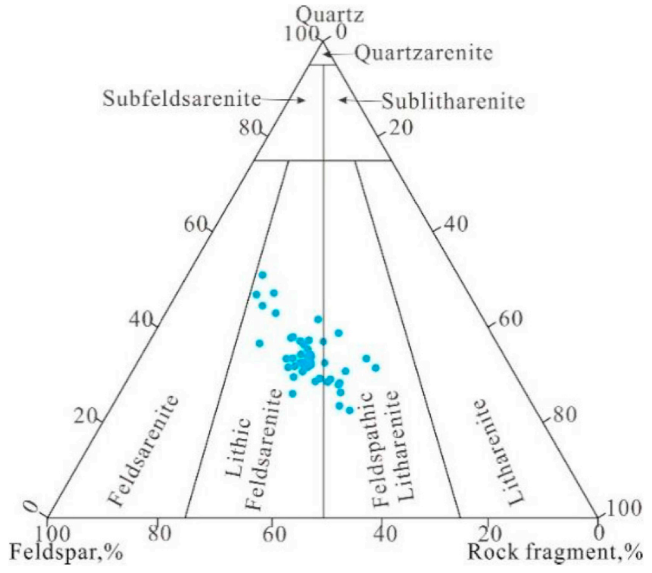

Fig. 4. Ternary plot showing the rock composition and rock types of the sandstones and pebbly sandstones in the Es4s in the Yanxie229 area (Folk et al., 1970). The contents of the rock composition were determined from the 46 thin sections.

Table 1
Rock composition derived from the 46 thin sections in the Es4s in the Yanxie229 area.

	Q/%	F/%	R/%	M/%	C/%	Cc/%	Otc/%
Max	40.2	36.0	39.0	15.0	19.3	17.5	5.98
Min	19.9	20.1	10.6	1.0	1.0	1.0	0
Ave	28.7	30.4	26.0	5.5	9.6	8.69	1.0

Q-Quartz; F-Feldspar; R-Rock fragment; M-Matrix; C-total content of Cements; Cc-Carbonate cements; Otc-other types of cements.

(ratio of (quartz) content/(feldspar + rock fragment) content) is 0.23–1.33 with an average of 0.55. The quartz grain content ranges from 19.9% to 40.2% with an average of 28.7%. The feldspar content ranges from 20.1% to 36% with an average of 30.4%. The rock fragment content ranges from 10.6% to 39% with an average of 26.0%. The cements include carbonates, quartz overgrowth, and authigenic clay minerals. The total cement content ranges from 1% to 19.3% with an average of 9.6%. The dominant cements are carbonate minerals. The total content of the carbonate cements ranges from 1% to 17.5% with an average of 8.69% (Table 1). The matrix content ranges from 1% to 15% with an average of 5.5% (Table 1).

4.2. Porosity and permeability

Primary intergranular pores, secondary dissolution pores and intercrystalline micropores in the kaolinite and carbonate cements are also observed in the oil layers in the Es4s reservoirs in the Yanxie229 area. The primary intergranular pores with straight margins (Fig. 5A) occur predominantly in the oil layers. The secondary pores are mainly formed by dissolution of feldspar grains (Fig. 5B) and carbonate cements (Fig. 5C). The secondary pores mainly include partial dissolution pores around the edges of the feldspar grains (Fig. 5B) and intragranular dissolution pores (Fig. 5D). The intercrystalline micropores of the kaolinites and carbonates are small (Fig. 5D).

The porosity and permeability of the reservoirs in the Es4s in the Yanxie229 area are in the ranges of 5%–10% and 1–10 mD, respectively (Fig. 6). There are dramatic differences in reservoir quality among the oil layers, water layers, and dry layers. The porosity and permeability range from 6.8% to 12.5% and from 1.4 mD to 10.1 mD, respectively in the oil layers (Fig. 7). The primary intergranular pores are the main reservoir spaces in the oil layers (Fig. 5A). Secondary dissolution pores and intercrystalline micropores of the kaolinites and carbonates are also observed in the oil layers (Fig. 5B, D). The porosity and permeability

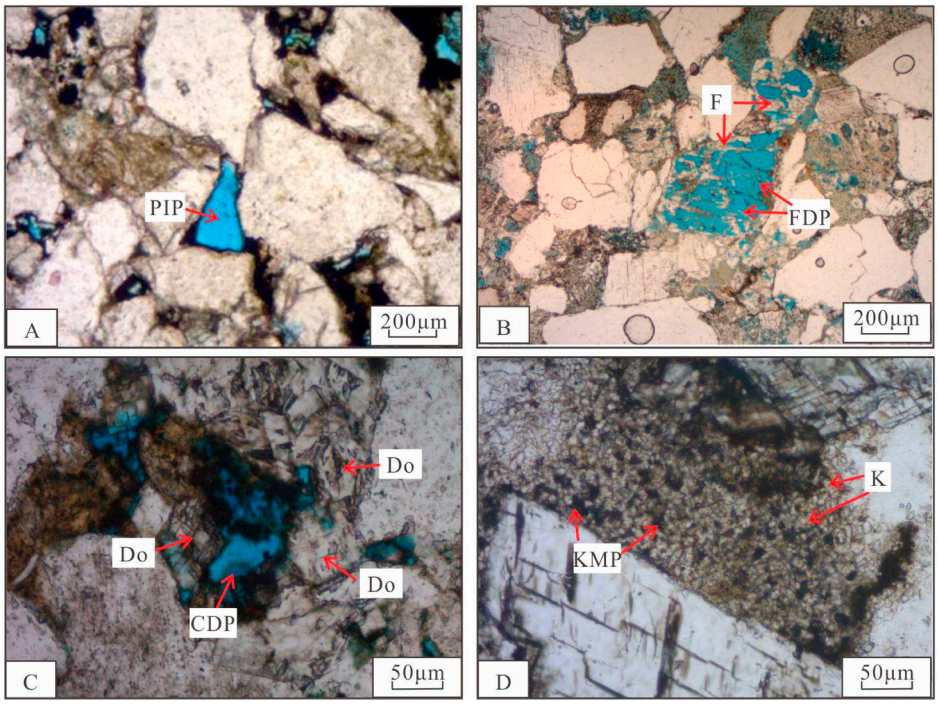

Fig. 5. Photomicrographs showing the pore characteristics of the reservoirs in the Es4s in the Yanxie229 area. (A) Well Yx229, 4148.5 m, oil layer, primary intergranular pores; (B) Well Yx232, 4140 m, oil-bearing water layer, dissolution pores of the feldspar grains; (C) Well Yx232, 4352 m, oil-bearing water layer, dissolution pores of the carbonate cements. (D) Well Yx232, 4000 m, oil layer, intercrystalline micropores within kaolinite crystal clusters. PIP-primary intergranular pore; F- feldspar; FDP- feldspar dissolution pore; Do-dolomite; CDP-carbonate dissolution pore; K-kaolinite; KMP-intercrystalline micropores of kaolinites.

range from 7.7% to 9.5% and from 2.7 mD to 6.9 mD, respectively in the oil-bearing water layers (Fig. 7). The dissolution pores are the main reservoir spaces in the water layers and oil-bearing water layers. The porosity and permeability in the dry layers are less than 5% and 1mD, respectively (Fig. 7). There are only a few micropores in the dry layers.

4.3. Diagenesis

4.3.1. Carbonate cementation

Carbonate cementation is the most common and dominant diagenesis type in the Es4s reservoirs in the Yanxie229 area. Cements of calcite, ferrocalcite, dolomite, and ankerite were detected (Plate 1).

The calcite cementation is uncommon. The calcites are red in the stained thin sections (Plate 1 A). The poikilotopic calcite cements were found only in one thin section, where the detrital grains are floating or have point contacts (Plate 1 A). The calcite cement emits bright yellow luminescence under the CL microscope (Plate 1 B). The calcite cement content is very low and nearly similar in the oil layers, oil-bearing layers, and dry layers (Fig. 9A). The calcite cement content ranges from 0% to 0.38% with an average of 0.11% in the oil layers, from 0.13% to 0.85% with an average of 0.4% in oil-bearing layers, and from 0% to 1.21% with an average of 0.3% in the dry layers (Fig. 9A).

The ferrocalcite cementation is also uncommon and weak. The ferrocalcites are purple in the stained thin sections (Plate 1 C). The ferrocalcite cements are mainly pore-filling blocky crystals. Ferrocalcite cement emits dark red luminescence under the CL microscope (Plate 1 D). The ferrocalcite cement content is low and nearly similar in the oil layers, oil-bearing layers, and dry layers (Fig. 9B). The ferrocalcite

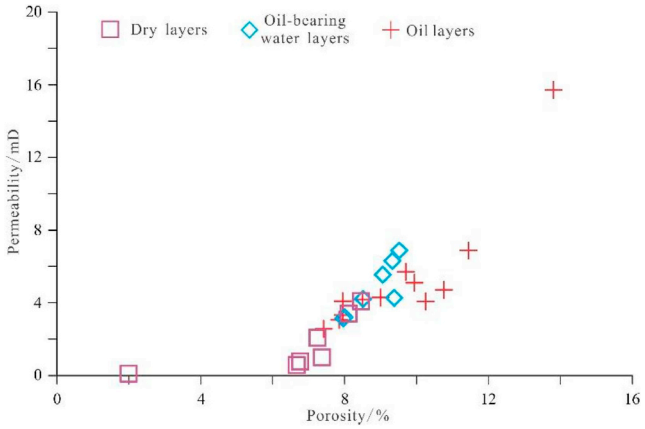

Fig. 7. Porosity and permeability of the oil layers, oil-bearing water layers, and dry layers in the Es4s in the Yanxie229 area. Each shape symbol represents one sample.

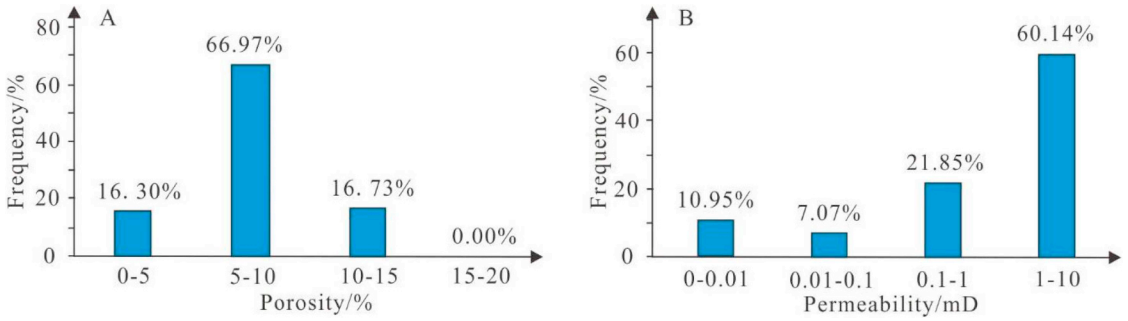

Fig. 6. Porosity and permeability of the reservoirs in the Es4s in the Yanxie229 area. (A) Histogram showing the distribution of porosity; (B) Histogram showing the distribution of permeability.

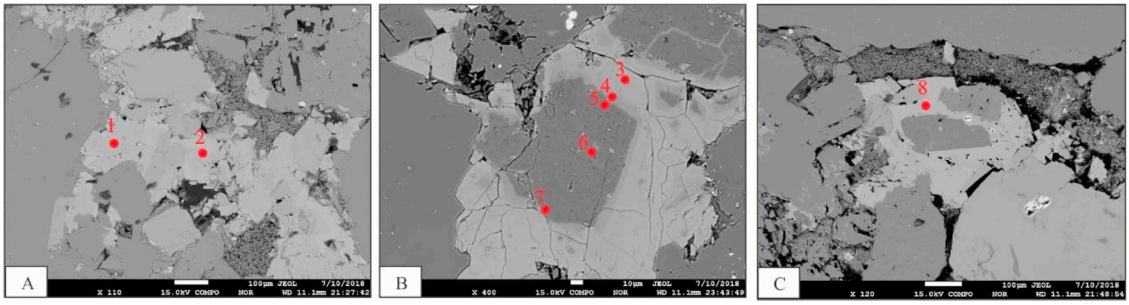

Fig. 8. Backscattered electron images (BSE) showing the characteristics of the carbonate cements and the positions and numbers of the EMPA in the Es4s reservoirs in the Yanxie229 area. (A) Well Y229-x1, 4179.3 m, pore-filling ankerites; (B) Well Yx232, 4031.5 m, pore-filling dolomites; (C) Well Yx232, 4031.5 m, ankerites with a dolomite grain inside.

cement content is higher than the calcite cement content. The ferrocalcite cement content ranges from 0% to 0.84% with an average of 0.20% in the oil layers, from 0% to 2.15% with an average of 0.94% in the oil-bearing layers, and from 0 to 1.65% with an average of 0.66% in the dry layers (Fig. 9B).

The dolomite cementation is more common than the ferrocalcite and calcite cementation. The dolomite cements are colorless in the stained thin sections (Plate 1 E) and emit light pink luminescence under CL (Plate 1 F). The results of the EMPA indicate that the cements consisting of MgO and CaO are probably dolomites (Table 2). The dolomite cements usually occur as pore-filling scattered euhedral crystals (Plate 1 E). The dolomite cements are relatively more abundant in the dry layers (Fig. 9C). However, the dolomite cement content is almost the same in the oil layers, oil-bearing water layers, and dry layers (Fig. 9C). The average content of the dolomite cements ranges predominantly from 2.5% to 5% (Fig. 9C).

The ankerite cementation is dominant in the E4s reservoirs in the Yanxie229 area. The ankerite cements are blue in the stained thin sections (Plate 1 G) and do not emit luminescence under CL (Plate 1 H). The results of the EMPA indicate that the cements consisting of FeO, MgO, and CaO are probably ankerites (Table 2). The ankerite cement content is markedly different in the oil layers, oil-bearing water layers, and dry layers (Fig. 9D). The ankerite cement content is lowest for the oil layers with an average of 0.92%, highest for the dry layers with an average of 7.57% and intermediate for the oil-bearing water layers with an average of 5.62%. The ankerite cements are more euhedral in the oil layer (Plate 1 I) than in the dry layers (Plate 1 G).

Replacements between different carbonate cements and quartz overgrowths also occurred in the Es4s reservoirs in the study area (Plate 1 C, J-L). Some of the ferrocalcite cements replaced the euhedral dolomite cements (Plate 1 C) and quartz overgrowths (Plate 1 J, K) and some of the ferrocalcite cements were replaced by the ankerite cements (Plate 1 L).

4.3.2. Quartz cementation and authigenic clay minerals

The quartz cementation is uncommon in the Es4s reservoirs in the Yanxie229 area. Only a small amount of quartz overgrowth was observed under the transmission and CL. The width of most of the quartz overgrowths is narrow (Fig. 10 A and B) with a few exceptions (Plate 1 J and K). The quartz overgrowth emits dark brown luminescence under CL (Fig. 10 B). Micro quartz was not detected under the SEM. Authigenic clay minerals are also uncommon. Only a small amount of authigenic kaolinite was found in some thin sections (Fig. 5 D). The content of the quartz overgrowth, micro quartz, and authigenic clay minerals was low in the Es4s reservoirs in the Yanxie229 area (Table 1).

4.3.3. Dissolution

Dissolution is weak in the Es4s reservoirs in the Yanxie229 area. A small amount of dissolution of the feldspar grains (Fig. 5B) and carbonate cements (Fig. 5C) can be observed in the thin sections of the oil layers and oil-bearing water layers. The pores created by the dissolution of minerals are not the dominant reason for the good reservoir quality of the Es4s reservoirs in the Yanxie229 area.

4.4. Fluorescent characteristics of oil and oil inclusions

The oil and carbonaceous bitumen in the intergranular pores and the adsorption in the matrix and cement can be distinguished under UV light. The oil emits yellow and blue fluorescence under UV light (Plate 2). Blue-fluorescent and yellow-fluorescent oil and oil inclusions occur in the Es4s reservoirs in the Yanxie229 area (Plate 2). In the oil-bearing water layers and dry layers, the yellow-fluorescent oil is dominant (Plate 2 A and B). In the oil layers, both blue- and yellow-fluorescent oil and oil inclusions (Plate 2 C to D) are found and the blue-fluorescent oil is dominant (Plate 2 C and D). Yellow- and blue-fluorescent oil inclusions exist independently (Plate 2E -H). No yellow- and blue-fluorescent oil inclusions are found simultaneously in the healed microfracture of quartz (Plate 2 F and H). Blue fluorescent oil inclusions do not show any stretching and cracking (Plate 2 G).

4.5. Fluid inclusions

4.5.1. Fluid inclusion petrography

Fluid inclusions could be divided into aqueous inclusions and oil inclusions depending on the presence of oil. Both aqueous inclusions and oil inclusions were developed in the Es4s reservoirs in the Yanxie229 area (Plate. 3, 4).

The oil inclusions are mostly light brown and colorless under plane-

Table 2
EMPA results of the chemical composition of the ankerites and dolomites in the Es4s reservoirs in the Yanxie229 area. See Fig. 8 for the positions and numbers of the EMPA.

Chemical composition	1	2	3	4	5	6	8
MgO	9.74 wt%	9.37 wt%	8.98 wt%	13.37 wt%	20.61 wt%	20.79 wt%	9.38 wt%
CaO	31.12 wt%	31.03 wt%	32.18 wt%	34.64 wt%	31.99 wt%	31.62 wt%	31.83 wt%
FeO	12.99 wt%	13.06 wt%	11.85 wt%	7.59 wt%	1.76 wt%	0.86 wt%	12.03 wt%
MnO	0.23 wt%	0.29 wt%	0.27 wt%	0.21 wt%	0.06 wt%	0.00 wt%	0.25 wt%
Carbonate type	ankerite	ankerite	ankerite	dolomite	dolomite	dolomite	ankerite

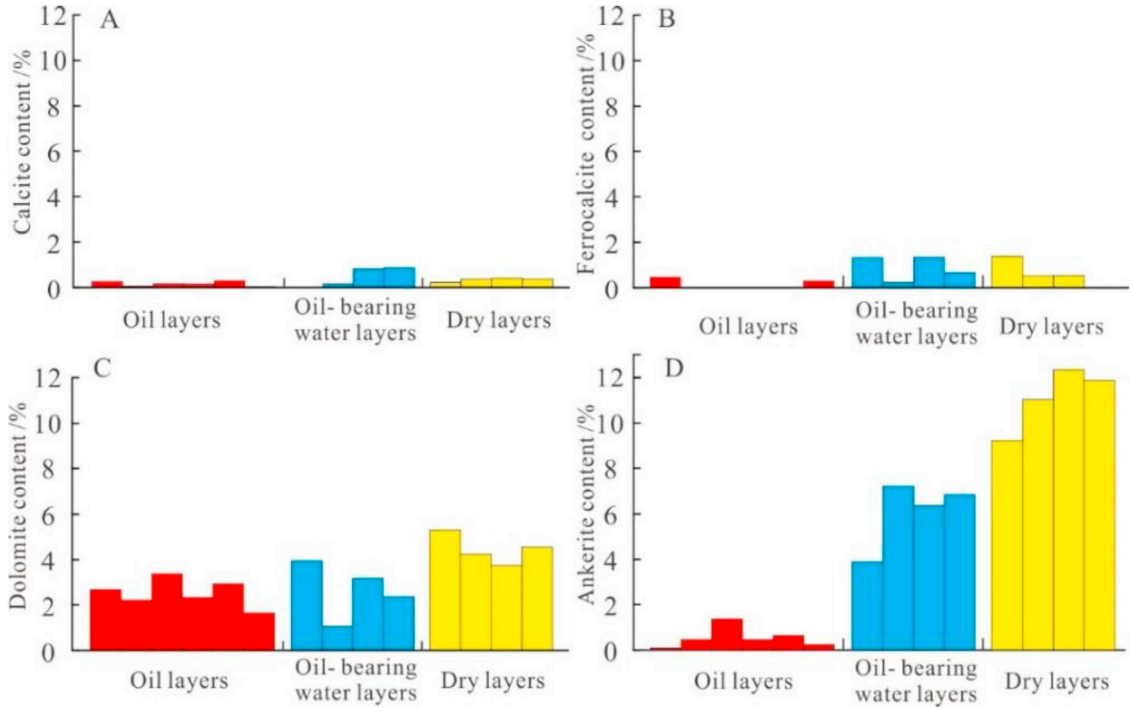

Fig. 9. Histograms showing the characteristics of the carbonate cement content in the oil layers, oil-bearing water layers, and dry layers in the Es4s in Yanxie229 area. (A)–(D) These histograms show the content of calcite, ferrocalcite, dolomite, and ankerite cements, respectively in the oil layers, oil-bearing water layers and dry layers.

polarized light and have two phases containing liquid (L) and vapor (V) at room temperature (Plate 3 A, C). The diameters along the maximum dimension of the oil inclusions range from 3 to 6 μm (Attached list 1). Oil inclusions emit yellow and blue fluorescence under UV light (Plate 3 B, D). Yellow- and blue-fluorescent oil inclusions in trails were dominantly distributed in the healed microfractures of the quartz grains (Plate 3 B, D). Yellow fluorescent oil inclusions also can be found in ankerite cement (Plate 4 M-O).

Aqueous inclusions are colorless under plane-polarized light (Plate 4 D, G), do not emit fluorescence under UV light (Plate 4 F, K), and have predominantly two phases containing L and V at room temperature (Plate 4 D-L). The diameters along the maximum dimension of the aqueous inclusions range from 3 to 7 μm (Attached list 1). Aqueous inclusions in trails are also common in the healed microfractures of the quartz grains (Plate 3 A). Two-phase aqueous inclusions are rare in the dolomite and ankerite cements (Plate 4 A-L). These inclusions are all tiny with a diameter of less than 6 μm (Plate 4 D, J). The two-phase aqueous inclusions in the dolomite cements, ankerite cements, and healed microfractures of quartz grains are nearly circular and do not show any signs of stretching or partial leakage (Plate 3, 4 A-L).

Fluid inclusions could be divided into primary, secondary, and pseudosecondary inclusions according to the origin (Goldstein, 2003). In each sample, the fluid inclusions were classified according to their morphology and relationship to the growth of the crystal. The aqueous and oil inclusions in the healed microfractures of quartz grains are secondary fluid inclusions because a single healed microfracture cuts across all growth zones of the overgrowth of quartz grains (Plate 3 A, C). The origin of the aqueous and oil inclusions in the dolomite and ankerite cements cannot be determined by observing the relationship to the growth of the crystal because the growth zones of the dolomite and ankerite cements are unclear (Plate 4 D, J). However, the aqueous and oil inclusions in the dolomite and ankerite cements are considered primary fluid inclusions because the two-phase aqueous inclusions in the dolomite and ankerite cements are nearly circular and do not show any signs of stretching or partial leakage (Plate 4 A-L). In addition, no fractures or deformation features are found near the aqueous inclusions (Plate 4 D, J).

Both single-phase oil inclusions and two-phase aqueous inclusions are developed in the same healed microfracture of the quartz grains (Plate 3 A, C), indicating that they are FIAs that were captured at the same time.

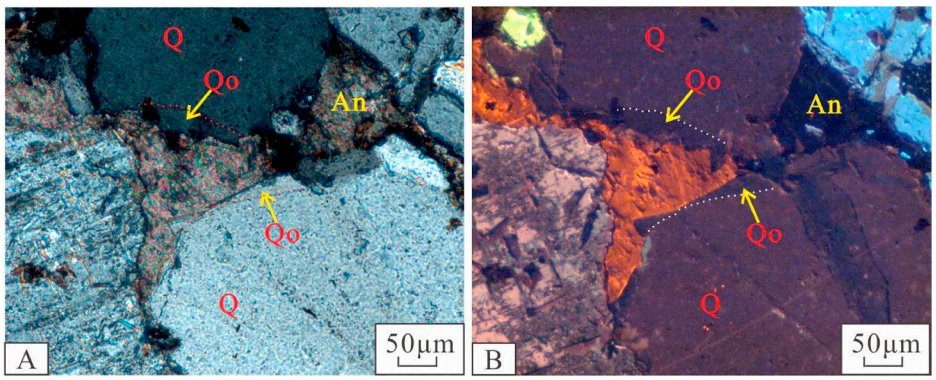

Fig. 10. Photomicrographs showing the characteristics of the quartz overgrowth in the Es4s reservoirs in the Yanxie229 area. (A) Well Yx232, 4256 m, characteristics of quartz overgrowth under cross-polarized light; (B) The same field view as A; the quartz overgrowth emits dark brown luminescence under CL. An-Ankerite; Q-quartz; Qo-quartz overgrowth.

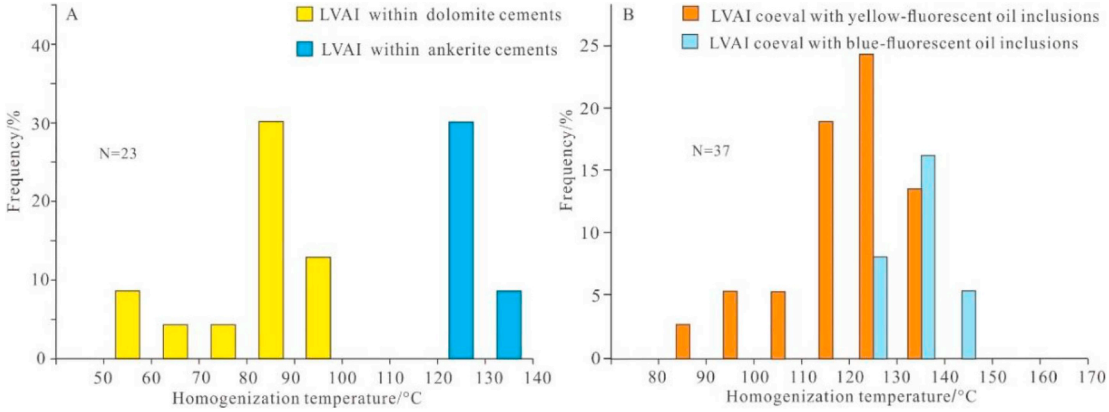

Fig. 11. Homogenization temperatures of the two-phase aqueous inclusions in the Es4s reservoirs in the Yanxie229 area. (A) Ths of the LVAIs in dolomite cements and ankerite cements; (B) Ths of the LVAIs coeval with oil inclusions.

4.5.2. Homogenization temperatures

The Ths of the two-phase aqueous inclusions in the dolomite cements range from 53.3 °C to 93.6 °C (Attached list 1) and the main peak of the Ths range from 80 °C to 90 °C (Fig. 11). Few aqueous inclusions occurred in the ankerite cements. Nine Ths of the two-phase aqueous inclusions in the ankerite cements were measured. The Ths of these 9 two-phase aqueous inclusions range from 123.8 °C to 135.5 °C with the main peak from 120 °C to 130 °C (Attached list 1; Fig. 11). The Ths of the two-phase aqueous inclusions coeval with the yellow-fluorescent oil inclusions range from 86.9 °C to 136.0 °C (Attached list 1) and the main peak ranges from 120 °C to 130 °C (Fig. 11). The Ths of the two-phase aqueous inclusions coeval with the blue-fluorescent oil inclusions range from 123.4 °C to 145.5 °C (Attached list 1) and the main peak ranges from 130 °C to 140 °C (Fig. 11).

4.6. YGOI and BGOI

The values of the YGOI and BGOI of the 14 samples were calculated (Attached list 2). The 14 samples include 6 samples from oil layers, 4 samples from oil-bearing water layers, and 4 samples from dry layers (Fig. 3; Table 3). The lithological characteristics of these selective 14 samples are very similar (Table 3) in order to minimize the influence of the rock composition on the calculation results of the YGOI and BGOI.

The YGOI values of the oil layer samples, oil-bearing water layer samples, and dry layer samples range from 27.98% to 46.12% with an average of 37.20%, from 8.83% to 33.02% with an average of 21.29%, and from 2.88% to 10.64% with an average of 5.88% (Attached list 2), respectively. The BGOI values of the oil layer samples, oil-bearing water layer samples, and dry layer samples range from 14.97% to 48.06% with an average of 26.32%, from 8.83% to 16.89% with an average of 12.56%, and from 1.18% to 5.96% with an average of 2.64% (Attached list 2), respectively.

5. Discussion

5.1. Sequence of oil emplacement and carbonate cementation

In order to understand the influence of oil emplacement on carbonate cementation in the case of multistage oil emplacement, it is essential to determine the sequence of oil emplacement and carbonate cementation (Worden and Morad, 2000; Bloch et al., 2002; Worden et al., 2018).

The precipitation temperatures of carbonate cements can be determined by the Ths of the two-phase aqueous inclusions in carbonate cements (Yuan et al., 2015; Wang et al., 2018) and can be calculated using oxygen stable isotope analysis (Friedman and O'Neil, 1977). The Ths of the two-phase aqueous inclusions in the dolomite and ankerite cements show that the dolomite and ankerite cements were precipitated

Table 3
Lithological data of the 8 core samples and the 6 typical side well coring samples of the pebbly sandstones in the Es4s in the Yanxie229 area. See Fig. 2 for the positions, numbers, and oiliness of the 14 samples. These 14 samples were used to calculate the values of the YGOI and BGOI.

N	Well	Depth/m	F/%	Q/%	RF/%	Mag/%	Meta/%	Cd/%	Mat/%	Otc/%	Sor	Rt	Ca/%	Do/%	Fc/%	An/%	Tc/%	PSo/%	O
1	Y229-x1	4175.7	25.2	29.7	25.1	4.2	20.9	0	5.5	0	5.65	PS	0.2	5.27	0.65	9.18	15.3	17.58	DL
2	Y229-x1	4175.95	26.2	31.6	24.2	5.2	15.5	3.5	4.1	0.2	5.78	PS	0.33	4.21	1.36	11	16.9	0	DL
3	Y229-x1	4176	28.4	30.3	24.7	5.1	17	3.2	4.5	1	5.66	PS	0.38	3.71	0.5	12.31	16.9	0	DL
4	Y229-x1	4179.3	27.3	26	30.2	7.2	19.3	3.7	6.4	5.98	4.28	PS	0.33	4.51	0.52	11.84	17.2	0	DL
5	Y229-x2	3753.45	30	34.5	28	14	14	0	4.5	0.06	4.59	PS	0.23	2.63	0	0.08	2.94	42.93	OL
6	Y229-x2	3754.9	30	35	25	9.5	11.9	3.6	6.9	0.01	4.92	PS	0.03	2.17	0.44	0.45	3.09	46.35	OL
7	Y229-x2	3755.85	30.5	32	28	8.8	19.2	0	4.5	0.06	4.58	PS	0.14	3.35	0	1.35	4.84	39.45	OL
8	Y229-x2	3759.1	32	35	27	3	22.5	1.5	3.2	0.26	4.59	PS	0.12	2.28	0	0.44	2.84	36.68	OL
9	Yx229	4132.5	31	33	26	5.2	15.6	5.2	2.1	0.11	6.49	PS	0.27	2.9	0	0.62	3.79	8.37	OL
10	Yx229	4148.5	35	30	30	12.5	16.2	1.3	3.1	0.07	5.36	PS	0	1.61	0	0.22	1.83	33.94	OL
11	Yx232	3987.2	30	32	27	9.9	15.7	2.4	3.9	0.04	5.27	PS	0	3.91	0.27	3.88	8.06	25.4	Obw
12	Yx232	4053.6	34	30	23	3.9	16.5	2.6	5.8	1.33	4	PS	0.13	1.02	1.31	7.18	9.64	11.23	Obw
13	Yx232	4110	31	33	22	14	6	1.8	3	0.56	4	PS	0.78	3.15	0.21	6.33	10.47	24.17	Obw
14	Yx232	4199.1	28	31	27	6.3	20.7	0	2.6	0.09	4.92	PS	0.85	2.33	1.32	6.81	11.31	32.62	Obw

N-number; Q-Quartz; F-Feldspar; RF-Rock fragment; Mag- Magmatite; Meta-Metamorphic rock; Cd-carbonate debris; Mat-Matrix; Otc-other types of cements; Sor-Sorting; Rt-Rock type; PS-Pebbly sandstone; Ca-calcite; Fc-Ferroan calcite; Do-Dolomite; An-Ankerite; Tc-total carbonate cement; PSo-Present oil saturation; O-Oiliness; WL-Dry layer; OL-Oil layer; Obw- Oil-bearing water layer; the oil and water saturation were interpreted by the Exploration and Development Research Institution of the Sinopec Shengli Oil field using well logging data. The contents of the rock composition and the rock texture data were obtained from the 14 thin sections.

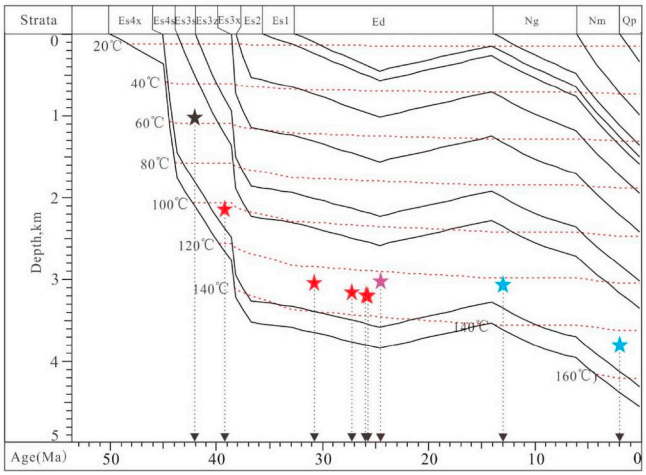

Fig. 12. Burial and thermal history plot of Well Yx229 showing the time of carbonate cement precipitation and hydrocarbon emplacement. The black five-pointed star represents the precipitation time of the dolomite cements. The red five-pointed star represents the time of yellow-fluorescent oil emplacement. The purple five-pointed star represents the time of the precipitation time of the ankerite cements. The blue five-pointed star represents the time of the blue-fluorescent oil emplacement. (For interpretation of the references to color in this figure legend, the reader is referred to the Web version of this article.)

at 53.3 °C–93.6 °C and at 123.8 °C–135.5 °C, respectively (Attached list 1). Ma et al. (2016) calculated the precipitation temperatures of calcite and ferrocalcite cements in the Es4s reservoirs in the Yanjia area using the oxygen isotope fractionation formulas of a calcite-water system (Kim and O'Neil, 1997) and dolomite-water water system (Horita, 2014). The calculation results showed that the calcite precipitation temperatures were at 28–41 °C and the ferrocalcite precipitation temperatures were 101–115 °C.

The fluid inclusions are not altered by contamination resulting from drilling and are unaffected by the time or conditions of storage. Crude oils with different chemical composition have different fluorescence colors. The fluorescence color reflects the difference in hydrocarbon inclusions and their thermal evolution. The fluorescence colors of oil the inclusions change with the increase in organic matter maturity (Stasiuk and Snowdon, 1997; Munz, 2001). Multi-phase filling of oil will lead to the appearance of oil inclusions with various fluorescence colors (Goldstein and Reynolds, 1994). Fluorescence colors may be used to determine the relative stage of oil emplacement.

Nevertheless, it is possible that the inclusions with different fluorescence colors may represent a single oil charge but the oil inclusions were trapped under slightly different conditions and/or on different grain surfaces (George et al., 2001); the yellow- and blue-fluorescent oil and oil inclusions in the study area (Plate 2; Plate 3 B, D) indeed represent two stages of oil emplacement. Firstly, there were two stages of oil generation in the source rocks in the study area (Guo et al., 2012) and two stages of oil emplacement into the reservoirs in the north zone of the Minfeng Subsag (Wang et al., 2016) where the study area is located (Fig. 1B). Secondly, it was found that yellow- and blue-fluorescent oil inclusions existed independently. No yellow- and blue-fluorescent oil inclusions were found simultaneously in the same healed microfracture of a quartz grain (Plate 2 F; Plate 3 D). Blue fluorescent oil inclusions did not show obvious stretching and cracking (Plate 3 B), which indicates that no secondary changes occurred in blue fluorescent oil inclusions. In addition, only yellow-fluorescent oil inclusions were found in the ankerite cement (Plate 4 M,O), indicating that yellow- and blue-fluorescent oil inclusions might not be formed during the same stage. Finally, the homogenization temperatures of aqueous inclusions coeval with yellow- and blue-fluorescent oil inclusions were significantly different. The Ths of the two-phase aqueous inclusions coeval with the yellow- and blue-fluorescent oil inclusions in the healed microfractures of quartz grains ranges from 86.9 °C to 136.0 °C and from 123.4 °C to 145.5 °C, respectively (Attached list 1).

The Ths of fluid inclusions reflect the reservoir temperature at the time when the fluid inclusions were captured (Karlsen et al., 1993; Goldstein, 2001; Parnell et al., 2001). The Ths of the hydrocarbon inclusions will change because organic matter may break down after entrapment (Qi et al., 2017; Ping et al., 2017). However, the aqueous inclusions coeval with the hydrocarbon inclusions have a higher stability of the Ths. The Ths of the two-phase aqueous inclusions coeval with the oil inclusions provide a more accurate representation of the formation temperatures when the hydrocarbon was emplaced into the reservoirs (Goldstein, 2001; Bourdet et al., 2012).

The Ths are assumed to be the minimum capture temperature of the aqueous inclusions. The Ths of aqueous inclusions were projected on the burial and thermal history plot of the corresponding well to obtain the sequence of oil emplacement and carbonate cementation. This method has been successfully applied to constrain the diagenetic history and the period of hydrocarbon emplacement in sedimentary rocks (Haszeldine et al., 1984; Mclimans, 1987; Goldstein, 2001; Liu et al., 2013) and has acceptable accuracy. Therefore, in this research, we used this method to obtain credible Ths of aqueous inclusions.

The primary two-phase aqueous inclusions (Plate 4 D, J) were used to measure the Ths. The consistent homogenization temperatures of the FIA indicate that the inclusions were not altered by thermal equilibration or necking and trapped miscible liquid and gas phases (Goldstein and Reynolds, 1994). The differences in the Ths of a single FIA were small. For example, the difference in the Ths of a single FIA in dolomite cement (Plate 4 D) was within 2 °C (Attached list 1). The Ths of aqueous inclusions in a microfracture of quartz (Plate 3 C) is similar (Attached list 1). During the repeated heating and cooling processes of the inclusions in the dolomite, ankerite cements, and healed microfractures of quartz grains, the volume of the vapor did not change when the inclusions cooled to room temperature after Th measurement. Therefore, the results of the homogenization temperature were credible. In order to determine the stage of hydrocarbon emplacement, the Ths of the two-phase aqueous inclusions coeval with the yellow- and blue-fluorescent inclusions were projected on the corresponding burial and thermal history plot using Well Yx229 as an example (Fig. 12). The results show that the emplacement of the first-stage yellow-fluorescent (FSYF) oil into the Es4s reservoirs occurred from about 41.5 Ma to 24.9 Ma and the emplacement of the second-stage blue-fluorescent (SSBF) oil into the Es4s reservoirs occurred from about 13 Ma to the present (Fig. 13 B). In order to determine the precipitation period of the carbonate cements, the precipitation temperatures of the calcite, dolomite, ferrocalcite, and ankerite cements were projected on the burial and thermal history plot (Fig. 12). The results show that the cements of the calcites, dolomites, ferrocalcites, and ankerites were dominantly precipitated in the periods from 43.8 Ma to 42.6 Ma, from 42.6 Ma to 38.7 Ma, from 27.8 Ma to 23.9 Ma, and from 24.2 Ma to 14.2 Ma (Fig. 13), respectively.

Based on the determined periods of multistage oil emplacement and different types of carbonate cementation, the sequence of oil emplacement and carbonate cementation was established (Fig. 13). Calcite cementation occurred first in the Es4s reservoirs in the study area. Dolomite cementation occurred slightly later than calcite cementation (Fig. 13 B). The ferrocalcite cementation occurred later than the dolomite cementation and earlier than the ankerite cementation (Fig. 13 B). The FSYF oil emplacement took place earlier than the ankerite cementation and later than the calcite cementation. Although the dolomite cementation and the FSYF emplacement overlapped for a short period, the predominant period of the FSYF oil emplacement was later than that of the dolomite cementation (Fig. 13 B). The period of ferrocalcite cementation was later than the predominant period of the FSYF oil emplacement (Fig. 13 B). The SSBF oil emplacement occurred later than all the carbonate cementation (Fig. 13 B).

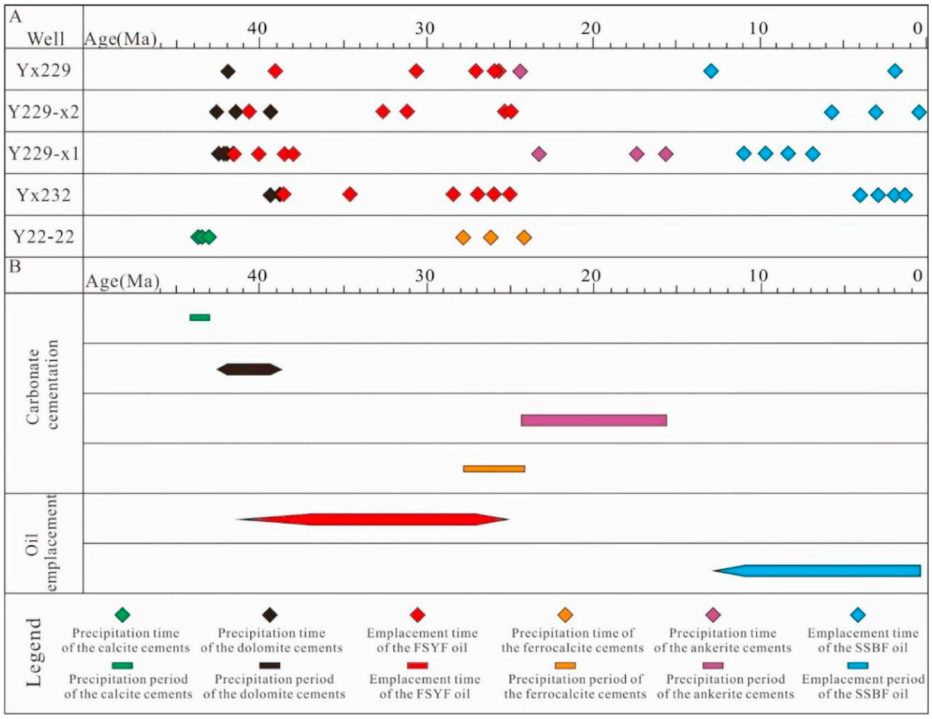

Fig. 13. (A). The time of carbonate cement precipitation and oil emplacement in the Es4s reservoirs in Wells Y229, Yx229-x2, Y229-x1, Yx232, and Y22-22. The green bar and orange solid diamonds represent the precipitation time of the calcite and ferrocalcite cements in the Es4s reservoirs in well Y22-22. The precipitation time of the calcite and ferrocalcite cements was determined based on the precipitation temperatures of the calcite and ferrocalcite cements calculated using oxygen isotope analysis as described by Ma et al., 2016. (B). Sequence of oil emplacement and carbonate cementation. The periods of the dolomite cementation, ankerite cementation, FSYF oil emplacement, and the SSBF oil emplacement were determined based on the specific precipitation time of the dolomite and ankerite cements and the specific emplacement time of the FSYF oil and the SSBF oil in (A). The periods of the calcite and ferrocalcite cementation were determined based on the precipitation time intervals in Y22-22 in (A), respectively. The width of the bar represents the strength of oil emplacement and carbonate cementation. (For interpretation of the references to color in this figure legend, the reader is referred to the Web version of this article.)

The periods of calcite and ferrocalcite cementation were determined by projecting the precipitation temperatures based on the oxygen stable isotopes on a burial and thermal history plot. There may be errors in determining the accurate periods of calcite and ferrocalcite cementation because the $\delta^{18}O_{SMOW}$ of the original formation water is difficult to measure accurately. However, the relative calculation error does not change the sequence of the two-stage oil emplacement and calcite and ferrocalcite cementation.

The replacement and cross-cutting relationship between different carbonate cements can also provide evidence for the sequence of oil emplacement and carbonate cementation. The ferrocalcite cements replaced the euhedral dolomite cements (Plate 1C) and quartz overgrowth (Plate 1J,K), which indicates that the ferrocalcite cementation occurred later than the dolomite cementation and quartz cementation. The Ths of the two-phase aqueous inclusions in the quartz overgrowth range from 118.7 °C to 135.4 °C (Attached list 1). The Ths of the two-phase aqueous inclusions coeval with the yellow-fluorescent oil inclusions range from 86.9 °C to 135.5 °C, which indicates that the precipitation time of the quartz overgrowth was almost coeval with the FSYF oil emplacement. As a result, the ferrocalcite cementation probably occurred later than the first-stage oil emplacement. The ferrocalcite cements were replaced by ankerite cements (Plate 1L), indicating that the ferrocalcite cementation took place earlier than the ankerite cementation and the SSBF oil emplacement.

Therefore the sequence of the two-stage oil emplacement and carbonate cementation in the Es4s reservoirs in the study areas is credible and the influence of the multistage oil emplacement on the carbonate cementation can be investigated further.

5.2. YGOI and BGOI reflecting paleo-oil saturation

Although it is very difficult to accurately determine paleo-oil saturation (Worden et al., 2018), the technique of GOI, which was developed by Eadington et al. (1996), efficiently determines the relative paleo-oil saturation (Lisk et al., 2002). The samples that have been exposed to high oil saturation have larger GOI values than the samples that have demonstrably low oil saturation (Lisk et al., 2002). The number of inclusions is a record of the continuous change in oil saturation in the reservoirs (Lisk et al., 2002). In most siliceous reservoirs, water is still the most important wetting phase; therefore, even increased oil saturation, diagenesis, and oil inclusion capture may continue, albeit at a slower rate (Walderhaug, 1994; Worden and Morad, 2003). Hence, the number of grains containing oil inclusions reflects the maximum paleo-oil saturation experienced in a sandstone reservoir irrespective of the present fluid phase (Lisk et al., 2002).

The GOI values reflect the paleo-oil saturation but the exact value cannot be determined (Eadington et al., 1996; Lisk et al., 2002). The GOI values are affected by the number of particles with oil inclusions therein. Except for oil saturation, the capture of oil inclusions can be influenced by many factors, such as the rate of mineral growth, the amount of crystal defects formed during mineral growth (Liu, 1979; Chen et al., 2011), the diagenetic fluid velocity (Prieto et al., 1996), and the wettability of the mineral surfaces (Chen et al., 2011). In addition, the GOI values decrease abnormally with a rapid increase in oil saturation caused by episodic oil emplacement because the oil inclusions are not captured in the diagenetic minerals in this case (George et al., 2004; Wang et al., 2005). For reservoirs with multistage oil emplacement, multistage emplaced oils have been superimposed. The oil saturation obtained from the actual cores will result in an incorrect understanding of the influence of multistage oil emplacement on carbonate cementation. It is necessary to obtain the paleo-oil saturation of each stage of oil emplacement in order to truly determine whether multistage oil emplacement exerted a control on carbonate cementation.

An attempt to obtain the relative paleo-oil saturation of each stage of multistage oil emplacement by calculating YGOI and BGOI was made in this research. However, the biodegradation, gas washing, water washing, mixed source, thermal cracking, and polar adsorption of crude oil during the capture period of oil inclusions should be taken into account because these processes cause oil inclusions to be stretched, leaked, or to contain bitumen adhering to the inclusion walls; this affects the changes in the fluorescence spectral parameters (George et al., 2001; Su et al., 2015). Therefore, these types of oil inclusions were all excluded during the calculation of the values of YGOI and BGOI.

The influence of the rock composition on the calculation results of the YGOI and BGOI was also excluded in this research by selecting

samples with similar lithological characteristics (Table 3). The Ths of the two-phase aqueous inclusions coeval with the FSYF oil inclusions are higher than 80 °C, which reaches the threshold temperature of quartz cementation (Walderhaug, 1994 Tingate and Rezaee, 1997). As a result, oil inclusions could be captured in the healed microfractures of the quartz grains during the two-stage oil emplacement in the Es4s reservoirs in the study area. The YGOI and BGOI values were calculated by only counting the water-wet quartz grains to exclude the influence of the wettability on the results. The Ths and time of oil emplacement were also relatively continuous (Fig. 13), indicating that the processes of oil emplacement were not episodic and rapid in the Es4s reservoirs in the Yanxie229 area.

The values of YGOI and BGOI were calculated (Attached list 2), excluding all the possible factors that may have resulted in an inaccurate evaluation of paleo-oil saturation. Only a small number of oil inclusions were eliminated during the process of counting the grains with the oil inclusions therein. Therefore, the values of YGOI and BGOI should be credible.

Previous research has suggested a GOI value of 5% as an empirical threshold for samples that have been exposed to high oil saturation, whereas values below 1% were likely to indicate only the migration of oil (Eadington et al., 1996; Lisk et al., 2002). The YGOI values of 2 samples from dry layers and the BGOI value of one sample from a dry layer were greater than 5% in the Es4s reservoirs in the Yanxie229 area. The values of YGOI and BGOI of all the samples from the oil-bearing water layers were greater than 5% in the Es4s reservoirs in the Yanxie229 area. A similar phenomenon was also found by Xie et al., 2007 in the Junggar Basin in China. The empirical threshold of 5% was used in the case of a single oil emplacement in a specific study area.

Except for oil saturation, the GOI values were also influenced by the other aforementioned factors. The BGOI values of the second-stage emplaced oil should be also impacted by the paleo-oil saturation of the first-stage emplaced oil. Therefore, the GOI thresholds for the oil layers and dry layers in the reservoirs with multi-stage oil emplacement should be redefined according to the specific geological background (Xie et al., 2007). Although the reason why the YGOI and BGOI values of the dry layers and oil-bearing water layers are greater than 5% and the specific threshold for the oil and dry layers are not clear in the Es4s reservoirs in the study area, in theory, the YGOI and BGOI values should reflect the level of paleo-oil saturation of the FSYF oil and the SSBF oil, respectively (Cao et al., 2007; Liu and Eadington, 2005).

5.3. Influence of the multistage oil emplacement on carbonate cementation

There is no correlation or a poor correlation between the content of total carbonate cements and the present oil saturation (Fig. 14 A) without considering the sequence of the two-stage oil emplacement and carbonate cementation in the Es4s reservoirs in the study area; this result appears to indicate that the influence of the two-stage oil emplacement on the carbonate cementation was extremely weak and negligible. In order to investigate whether the two-stage oil emplacement exerted influences on the carbonate cementation, the dolomite and ankerite cements were selected considering that they represented a large proportion (Fig. 9 C and D) and the relatively accurate sequence of the two-stage oil emplacement and the dolomite and ankerite cementation (Figs. 15 and 16). The calcite cements and ferrocalcite cements were not selected due to their low content (Fig. 9 A).

In addition to oil emplacement, diagenesis and reservoir quality are also related to other factors (Worden et al., 1998; Worden and Morad., 2000; Taylor et al., 2010; Meng et al., 2010). In order to eliminate the influence of the rock composition and texture on the carbonate cementation and reservoir quality, 14 samples of pebbly sandstones with very similarly lithological characteristics were selected (Table 3). No microcrystalline quartz and authigenic clay coatings were found on the grain surfaces in the Es4s reservoirs in the Yanxie229 area. Therefore, it is reasonable and credible that the differences in the dolomite and ankerite cement contents were principally caused by the multistage oil emplacement in the Es4s reservoirs in the Yanxie229 area.

There are no or poor negative correlations between the content of the dolomite cements, the present oil saturation, YGOI, and BGOI (Figs. 14 B, Fig. 15 A, B), indicating that the two-stage oil emplacement had no effect on the dolomite cementation. The dolomite cementation occurred earlier than the FSYF oil emplacement and the SSBF oil emplacement (Fig. 13 B). As a result, it is reasonable to conclude that there was no influence of the two-stage oil emplacement on the dolomite cementation. Therefore, there was almost no difference in the dolomite cement contents between the oil layers, oil-bearing water layers, and dry layers (Fig. 9 C).

The close negative correlation between the YGOI and the ankerite cement content (Fig. 15 C) indicate that the ankerite cementation was significantly inhibited by the FSYF oil emplacement. The emplacement of the FSYF oil into the Es4s reservoirs occurred earlier than the ankerite cementation (Fig. 13 B). The relative permeability of the water phase gradually decreased with the emplacement of the FSYF oil into the Es4s reservoirs, which resulted in a decrease in the transportation rate of Ca^{2+}, Mg^{2+}, and CO_3^{2-} because these ions were predominantly derived from the adjacent mudstones by advection in deep clastic reservoirs (Wang et al., 2014; Xi et al., 2015b; Yang et al., 2017). As a result, the transportation of the fluid saturated with calcium carbonate into the Es4s reservoirs was probably inhibited in the case of high oil saturation (Worden et al., 1998; Taylor et al., 2010; Bukar, 2013; Neveux et al., 2014). Therefore, the ankerite cementation was effectively inhibited by the FSYF oil emplacement and the degree of inhibition increased with the increase in the paleo-oil saturation of the FSYF oil (YGOI). The ankerite cement content was less than 2% in the oil layers when the YGOI values were higher than 30%. The close positive correlation between YGOI and porosity (Fig. 16 A) and the larger number of primary and secondary pores in the oil layers also suggests that the FSYF oil emplacement inhibited the ankerite cementation and preserved the Es4s reservoirs from being destroyed by the ankerite

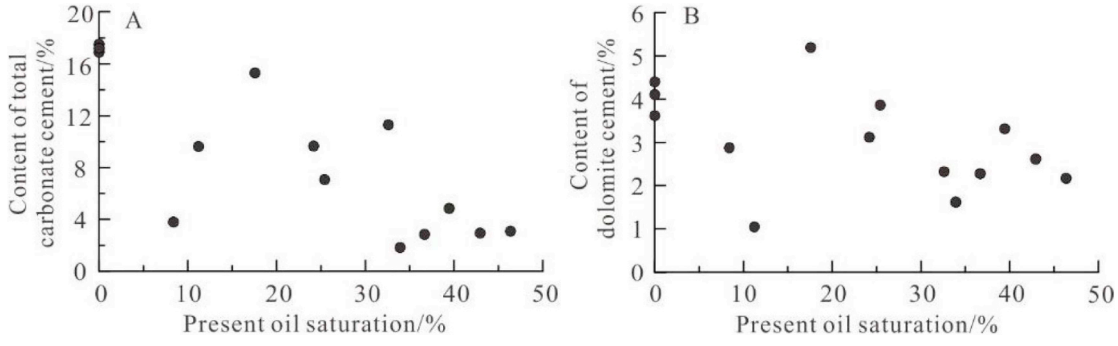

Fig. 14. (A) Relationship between present oil saturation and content of total carbonate cements. (B) Relationship between present oil saturation and dolomite cements.

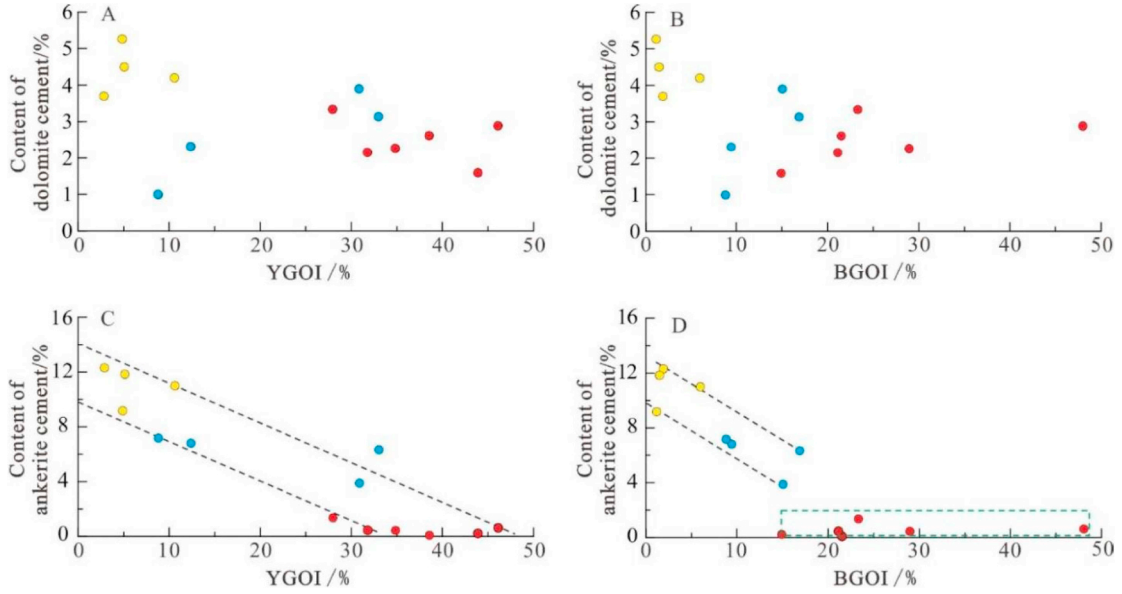

Fig. 15. Relationships among YGOI, BGOI, and the dolomite and ankerite cement content in the Es4s reservoirs in the Yanxie229 area. The yellow, blue, and red solid circles represent the dry layers, oil-bearing water layers, and oil layers, respectively. (For interpretation of the references to color in this figure legend, the reader is referred to the Web version of this article.)

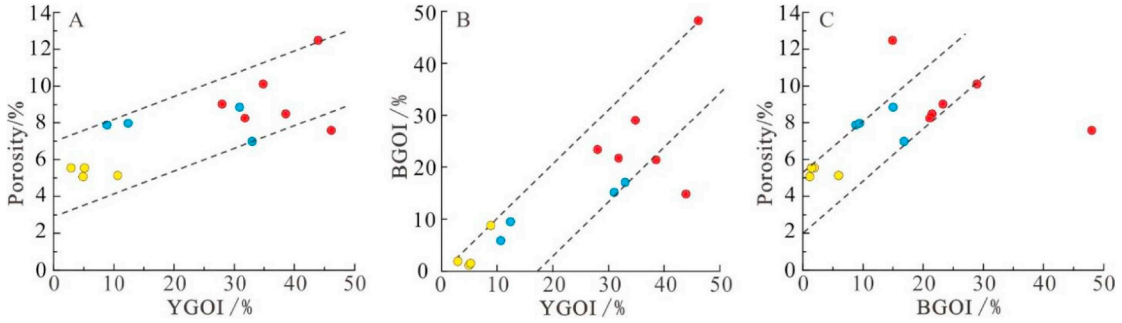

Fig. 16. Relationship between YGOI and BGOI and between YGOI and porosity in the Es4s reservoirs in the Yanxie229 area.

cementation.

There was a close negative correlation between the BGOI and the ankerite content when the ankerite cement content was more than 2% (Fig. 15 D), suggesting that the ankerite cementation appeared to be inhibited by the SSBF oil emplacement. In fact, the inhibition was not caused by the SSBF oil emplacement. The reservoirs with ankerite cement contents of more than 2% are dry layers and oil-bearing water layers (Fig. 16 D). The present-day formation temperatures ranged from 142 °C to 151 °C in Well Yx229 and Well Yx232, where the samples of the dry layers were taken. The Ths (123.5 °C–138.8 °C) of the two-phase aqueous inclusions in the ankerite cements in these dry layers (Table 3) were lower than the present-day formation temperatures. The ankerite cementation occurred earlier than the SSBF oil emplacement (Fig. 13).

The low content of the SSBF oil (Plate 2 C, D) and the BGOI values less than 15% (Fig. 15D) suggest that small amounts of the SSBF oil were emplaced into the dry layers and oil-bearing water layers. Most pores in the dry layers and oil-bearing water layers were damaged by ankerite cementation (Fig. 5G). In particular, only a few micropores were preserved in the dry layers (Fig. 7). The intense ankerite cementation had occurred in the dry layers prior to the emplacement of the SSBF oil into the Es4s reservoirs because it lacked the protection of the FSYF oil emplacement, which resulted in a small number of pores being preserved prior to the SSBF oil emplacement. Consequently, the second-stage oil could not easily charge into the Es4s reservoirs, which resulted in the low BGOI values in the dry layers (Fig. 15 D). Therefore, the ankerite cementation in the dry layers and oil-bearing water layers was inhibited or stopped not because of the SSBF oil emplacement but because of the significant destruction of the pores and the reduction in the transportation rate of the external material by the intense ankerite cementation prior to the SSBF oil emplacement.

There was no correlation between the BGOI and the ankerite cement content in the oil layers when the ankerite cement content was less than 2% and the BGOI values were greater than 15% (Fig. 15D); this indicated that the ankerite cementation was not inhibited by the SSBF oil emplacement. However, the ankerite cementation occurred later than the FSYF oil emplacement and earlier than the SSBF oil emplacement (Fig. 13). The Th (124.2 °C) of the two-phase aqueous inclusions in the ankerite cements in the oil layers (Attached list 1) was similar to the Ths (123.5 °C–138.8 °C) of the two-phase aqueous inclusions in the ankerite cements in the dry layers; this temperature was lower than the present-day formation temperatures. These results indicate that the ankerite cementation continued slowly in the oil layers where the FSYF oil had been effectively accumulated if the SSBF oil was not emplaced into these oil layers. Consequently, in essence, the SSBF oil

emplacement increased the paleo-oil saturation in the oil layers and basically stopped the ankerite cementation.

The porosity increased with the increase in the BGOI values except for two abnormal points (Fig. 14 C), also suggesting that the SSBF oil emplacement did preserve the reservoir quality. The close positive correlation between YGOI and BGOI (Fig. 16 B) and the larger amount of SSBF oil than FSYF oil in the oil layers (Plate 3 A and B) suggest that the SSBF oil was more likely to be accumulated in the reservoirs where the FSYF oil had been accumulated. The FSYF oil emplacement inhibited the ankerite cementation and preserved the porosity, which reduced the migration resistance of the SSBF oil. The FSYF oil emplacement probably changed the wettability of the reservoirs from water-wet to oil-wet (Hielmeland and Larrondo, 1986; Robin et al., 1995). The oil-wet ankerite cements also reduced the flow resistance of the SSBF oil (Toledo et al., 1996; Zhang et al., 2007). As a result, the SSBF oil was more easily emplaced into the reservoirs where the FSYF oil was accumulated. Yan et al. (2012) also proposed that the later oil would prefer to migrate along the pathways where the FSYF oil migration had occurred. Therefore, the ankerite cementation was dominantly inhibited by the FSYF oil. The SSBF oil emplacement played a significant role in the further increase in paleo-oil saturation, which enhanced the inhibition of the ankerite cementation and even stopped it in the oil layers.

6. Conclusions

The determination of the sequence of oil emplacement and carbonate cementation is crucial to understand the influence of oil emplacement on carbonate cementation against the geological background of multistage oil emplacement and carbonate cementation. If the sequence of oil emplacement and carbonate cementation is not considered, it is likely that misleading conclusions will be drawn.

The emplacement of the FSYF oil into the Es4s reservoirs in the study area occurred earlier than the ankerite cementation and ferrocalcite cementation but later than the calcite cementation and dolomite cementation. The emplacement of the SSBF oil into the Es4s reservoirs in the study area occurred later than all the carbonate cementation. The dolomite cementation was not influenced by the FSYF oil emplacement in the Es4s reservoirs in the study area because the dolomite cementation had stopped before the FSYF oil emplacement occurred. The ankerite cementation was dominantly inhibited by the FSYF oil emplacement in the Es4s oil layers. The SSBF oil emplacement played a significant role in the further increase in paleo-oil saturation, which enhanced the inhibition of the ankerite cementation and even stopped it in the Es4s oil layers.

Acknowledgment

This research was co-funded by the National Natural Science Foundation of China (Grant No. 41772137), the National Science and Technology Major Project (2016ZX05006-003-003), and the Fundamental Research Funds for the Central Universities (17CX05009). We would like to thank Shengli Oilfield Company of SINOPEC for providing core samples, side well coring samples, logging data, and porosity and permeability data.

Appendix A

Attached list 1

Homogenization temperatures and sizes of the two-phase aqueous inclusions in the Es4s reservoirs in the Yanxie229 area.

N	Well	Depth, m	Size, μm	Th/°C	Host mineral	Fc	N	Well	Depth, m	Size, μm	Th/°C	Host mineral	Fc
1	Y229-x2	3253.45	5.64	53.3	Do	–	31	Yx229	4179.3	3.09	145.5	Hmq	B
2	Yx229	4307	3.22	59.7	Do	–	32	Y229-x2	3755.85	4.18	124.3	Hmq	B
3	Y229-x2	3253.45	4.51	68.2	Do	–	33	Y229-x2	3755.85	3.91	142.8	Hmq	B
4	Y229-x2	3253.45	5.83	70.6	Do	–	34	Y229-x2	3755.85	6.67	133.4	Hmq	B
5	Y229-x1	4175.3	3.81	81.2	Do	–	35	Yx232	4350.2	6.35	125.3	Hmq	Y
6	Y229-x1	4175.3	4.58	87.3	Do	–	36	Yx232	4350.2	4.21	118.6	Hmq	Y
7	Yx232	4224	5.47	88.5	Do	–	37	Y229-x1	4175.7	3.78	112.8	Hmq	Y
8	Y229-x1	4175.3	4.26	88.5	Do	–	38	Y229-x2	3254.9	5.33	86.9	Hmq	Y
9	Yx232	4366	3.45	88.6	Do	–	39	Yx229	4179.3	3.85	125.2	Hmq	Y
10	Y229-x1	4175.3	4.51	92.5	Do	–	40	Yx229	4179.3	5.46	131.1	Hmq	Y
11	Y229-x2	3253.45	3.71	93.6	Do	–	41	Yx229	4179.3	3.61	103.4	Hmq	Y
12	Y229-x2	3754.9	4.23	83.5	Do	–	42	Yx229	4179.3	2.82	136	Hmq	Y
13	Y229-x2	3754.9	3.98	87.1	Do	–	43	Yx229	4179.3	5.57	131.8	Hmq	Y
14	Y229-x1	4175.7	5.23	90.1	Do	–	44	Y229-x2	3755.85	4.65	116.7	Hmq	Y
15	Y229-x1	4175.95	5.2	123.8	An	–	45	Y229-x2	3755.85	5.45	114.8	Hmq	Y
16	Yx229	4179.3	5.81	124.2	An	–	46	Y229-x2	3755.85	4.44	132.3	Hmq	Y
17	Y229-x1	4175.95	3.83	126.2	An	–	47	Y229-x2	3755.85	4.45	121.6	Hmq	Y
18	Y229-x1	4175.95	4.37	135.5	An	–	48	Y229-x1	4175.95	4.81	126.4	Hmq	Y
19	Y229-x2	3755.85	2.73	125.9	An	–	49	Y229-x1	4175.7	3.56	126.1	Hmq	Y
20	Y229-x2	3755.85	3.35	126.7	An	–	50	Yx232	4350.2	4.36	93.7	Hmq	Y
21	Y229-x2	3755.85	3.62	125.8	An	–	51	Yx232	4350.2	3.18	135.5	Hmq	Y
22	Y229-x1	4175.3	3.41	136.3	An	–	52	Yx232	4350.2	2.55	115.8	Hmq	Y
23	Y229-x2	3754.9	2.85	129.5	An	–	53	Yx232	4350.2	3.69	103.5	Hmq	Y
24	Y229-x1	4175.7	5.36	131.8	Hmq	B	54	Y229-x1	4175.7	3.7	93.6	Hmq	Y
25	Y229-x1	4175.7	5.12	130.6	Hmq	B	55	Y229-x1	4175.7	3.78	112.8	Hmq	Y
26	Y229-x1	4175.7	4.26	138.3	Hmq	B	56	Yx232	4224	2.48	135.4	Qo	Y
27	Y229-x1	4175.7	3.44	136.5	Hmq	B	57	Yx232	4224	3.42	118.7	Qo	Y
28	Yx232	4224	3.06	125	Hmq	B	58	Yx232	4224	4.12	124.8	Qo	Y
29	Yx232	4224	6.21	130.2	Hmq	B	59	Y229-x2	3755.85	3.65	121.6	Qo	Y
30	Yx229	4179.3	5.78	123.4	Hmq	B	60	Y229-x2	3755.85	4.12	132.4	Qo	Y

Abbreviation: Th-homogenization temperature; Hmq-healed microfracture of a quartz grain; Do-dolomite cement; An-ankerite cement; Qo-quartz overgrowth; Fc-fluorescence color of the hydrocarbon inclusions coeval with two-phase aqueous inclusions; B-blue fluorescence; Y-yellow fluorescence.

Attached list 2

Values of YGOI and BGOI in the Es4s reservoirs in the Yanxie229 area. See Fig. 2 for the positions, numbers, and oiliness of the 14 samples.

N	Well	Depth/m	NQG	NQYG	NQBG	YGOI	BGOI	Oiliness
1	Y229-x1	4175.7	677	33	8	4.87%	1.18%	DL
2	Y229-x1	4175.95	235	25	14	10.64%	5.96%	DL
3	Y229-x1	4176	208	6	4	2.88%	1.92%	DL
4	Y229-x1	4179.3	665	34	10	5.11%	1.50%	DL
5	Y229-x2	3753.45	604	233	130	38.58%	21.52%	OL
6	Y229-x2	3754.9	582	185	123	31.79%	21.13%	OL
7	Y229-x2	3755.85	386	108	90	27.98%	23.32%	OL
8	Y229-x2	3759.1	442	154	128	34.84%	28.96%	OL
9	Yx229	4132.5	464	214	223	46.12%	48.06%	OL
10	Yx229	4148.5	835	367	125	43.95%	14.97%	OL
11	Yx232	3987.2	259	80	39	30.89%	15.06%	Obw
12	Yx232	4053.6	691	61	61	8.83%	8.83%	Obw
13	Yx232	4110	527	174	89	33.02%	16.89%	Obw
14	Yx232	4199.1	508	63	48	12.40%	9.45%	Obw

Annotation: NQG: Total number of quartz grains counted; NQYG: number of quartz grains with yellow-fluorescent oil inclusions; NQBG: number of quartz grains with blue-fluorescent inclusions; YGOI: the ratio of the number of quartz grains with yellow-fluorescent oil inclusions therein to the NQG; BGOI: the ratio of the number of quartz grains with blue-fluorescent oil inclusions therein to the NQG. OL: Oil layer; Obw: Oil-bearing water layer; DL: Dry layer.

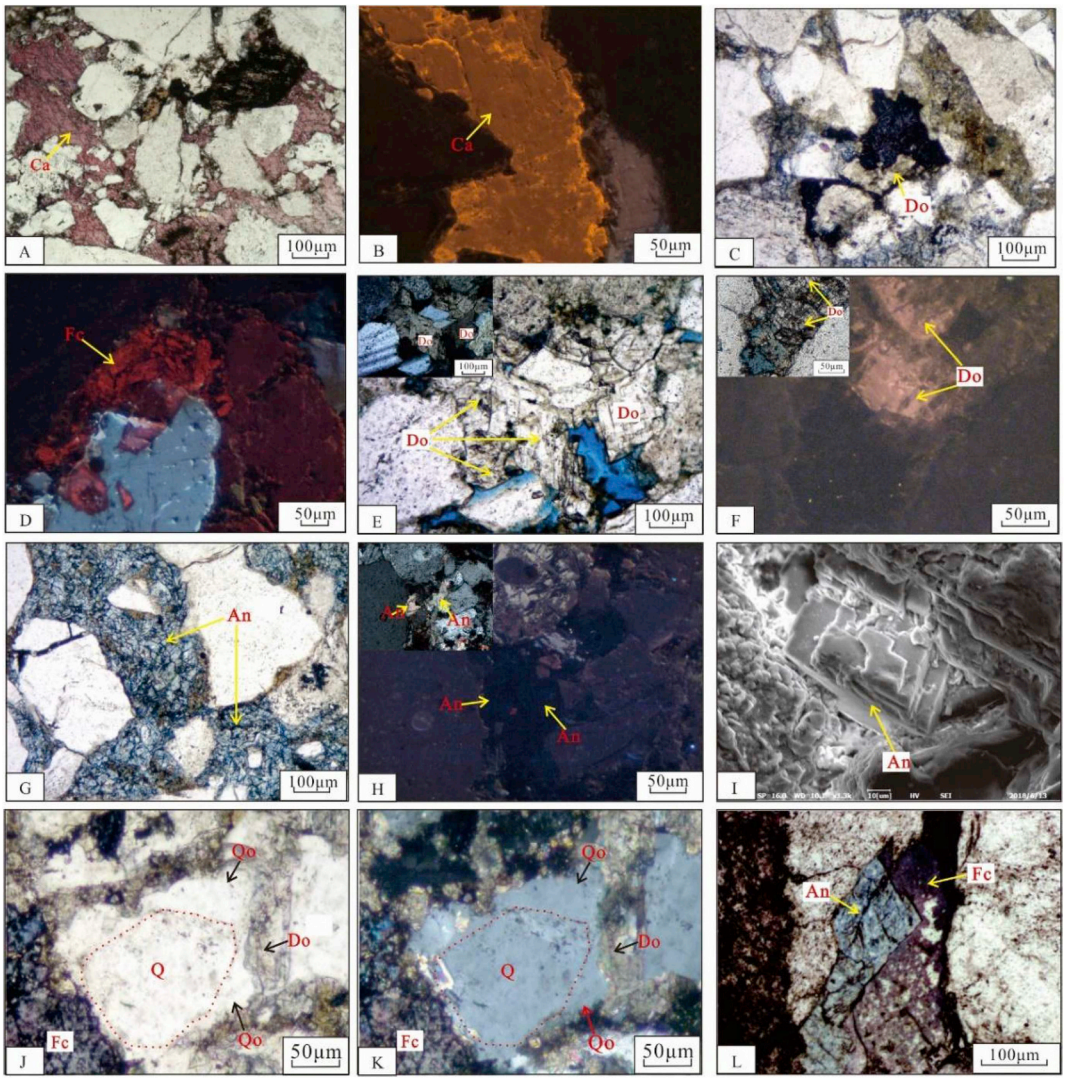

Plate 1. Photomicrographs showing the characteristics of the carbonate cementation in the Es4s reservoirs in the Yanxie229 area. (A) Well Yx229, 4098 m, oil layer, red calcites in stained thin section; (B) Well Yx233, 3788 m, dry layer, calcites emit yellow luminescence under CL; (C) Well Yx229, 4098 m, oil layer, pore-filling ferrocalcite is purple in stained thin section and dolomite is colorless; the dolomite was replaced by ferrocalcite; (D) Well Yx232, 4091.7 m, oil-bearing water layer, ferrocalcite emit dark red luminescence under CL; (E) Well Yx232, 4352 m, oil layer, discrete euhedral dolomite cements in stained thin section; (F) Well Y229-x1, 4179.3 m, dry layer, dolomite cements emit light pink luminescence under CL; (G) Well Yx233, 3536.6 m, dry layer, poikilotopic blue ankerite in stained thin section; (H) Well Y229-x1, 4179.3 m, dry layer, ankerite without luminescence under CL; (I) Well Yx229, 4148.5 m, oil layers, euhedral ankerite under SEM; (J) Well Yx233, 3536.6 m, purple ferrocalcite and colorless dolomite in stained thin section, quartz overgrowth was replaced by ferrocalcite and dolomite, plane-polarized light; (K) The same field view as J under cross-polarized light; (L) Well Yx232, 4199.1 m, purple ferrocalcite and blue ankerite in stained thin section; the ferrocalcite was replaced by ankerite. Ca-calcite; Fc-Ferroancalcite; Do-Dolomite; An-Ankerite; Q-quartz; Qo-quartz overgrowth.

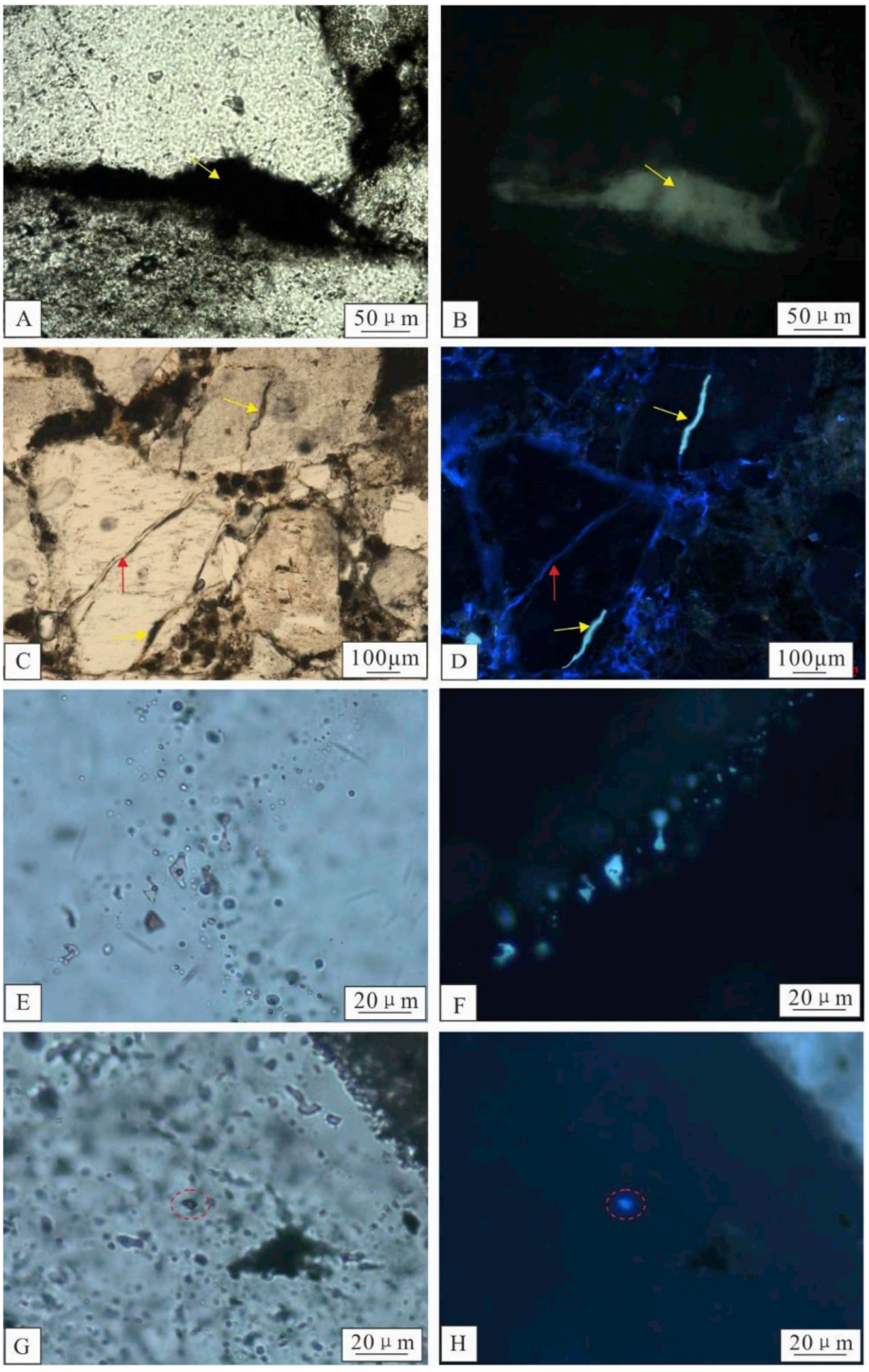

Plate 2. Photomicrographs showing the fluorescent characteristics of the oil and oil inclusions in the oil layers, oil-bearing water layers, and dry layers in the Es4s reservoirs in the Yanxie229 area. (A) Well Yx232, 4000 m, oil-bearing water layer, under plan-polarized light. (B) The same field view as (A), under ultraviolet light, oil emits yellow fluorescence (yellow arrow). (C) Well Y229-x2, 3754.9 m, oil layer, under plan-polarized light. (D) The same field view as (C), under ultraviolet light, oil emits yellow (yellow arrow) and blue fluorescence (red arrow). (E) Well Y229-x2, 3759.1 m, oil layer, under plan-polarized light. (F) The same field view as (E), under ultraviolet light, oil inclusions in the healed microfracture of quartz emit yellow fluorescence. (G) Well Y229-x2, 3754.9 m, oil layer, under plan-polarized light. (H) The same field view as (G), under ultraviolet light, oil inclusions in quartz grains emit blue fluorescence.

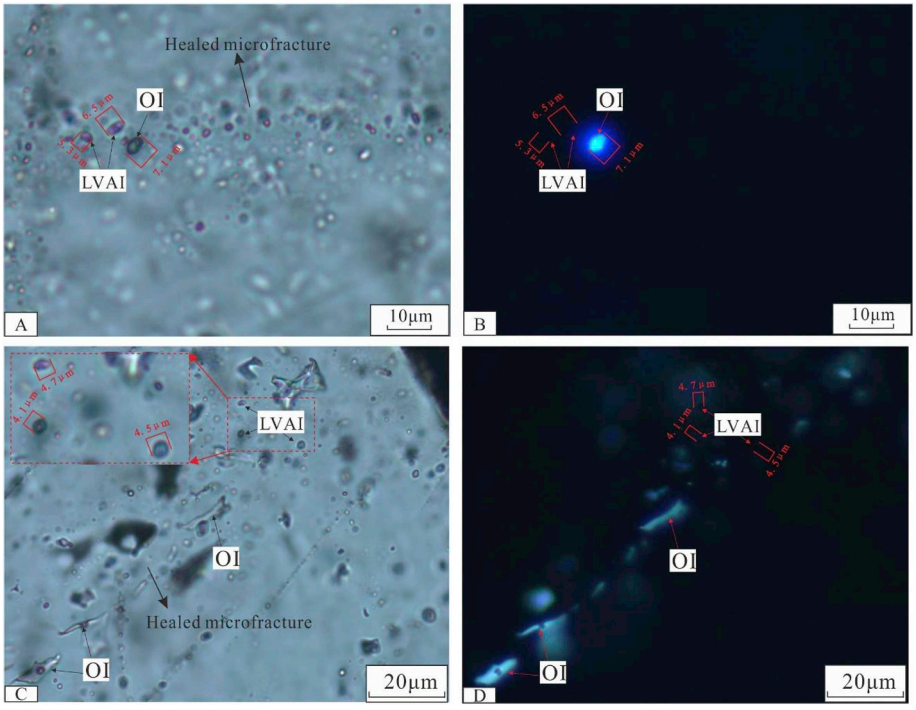

Plate 3. Photomicrographs of oil inclusions and aqueous inclusions trapped in healed microfractures of quartz grains in the Es4s reservoirs in the Yanxie229 area. (A) Well Yx2322, 3286 m, two-phase (L + V) aqueous inclusions (LVAI) coeval with single-phase oil inclusions in a healed microfracture of a quartz grain. Both the aqueous and oil inclusions are colorless under plane polarized light. The pink color of the magnified oil inclusions is the result of the refractive indices of the fluid inclusion and host mineral (Kerkhof and Hein, 2001). (B) the same field view as (A), single-phase blue-fluorescent oil inclusions and two-phase aqueous inclusions coeval with the single-phase blue-fluorescent oil inclusions; the oil inclusions emit blue fluorescence and the two-phase aqueous inclusions do not emit fluorescence under ultraviolet light. (C) Well Y229-x2, 3759.1 m, the two-phase aqueous inclusions coeval with single-phase oil inclusions in a healed microfracture of a quartz grain. Both the aqueous and hydrocarbon inclusions are colorless under plane polarized light; (D) the same view as (C); the single-phase oil inclusions emit yellow fluorescence under ultraviolet light. The two-phase aqueous inclusions coeval with the single-phase oil inclusions do not emit fluorescence; LVAI-two-phase (L + V) aqueous inclusion; OI-oil inclusion.

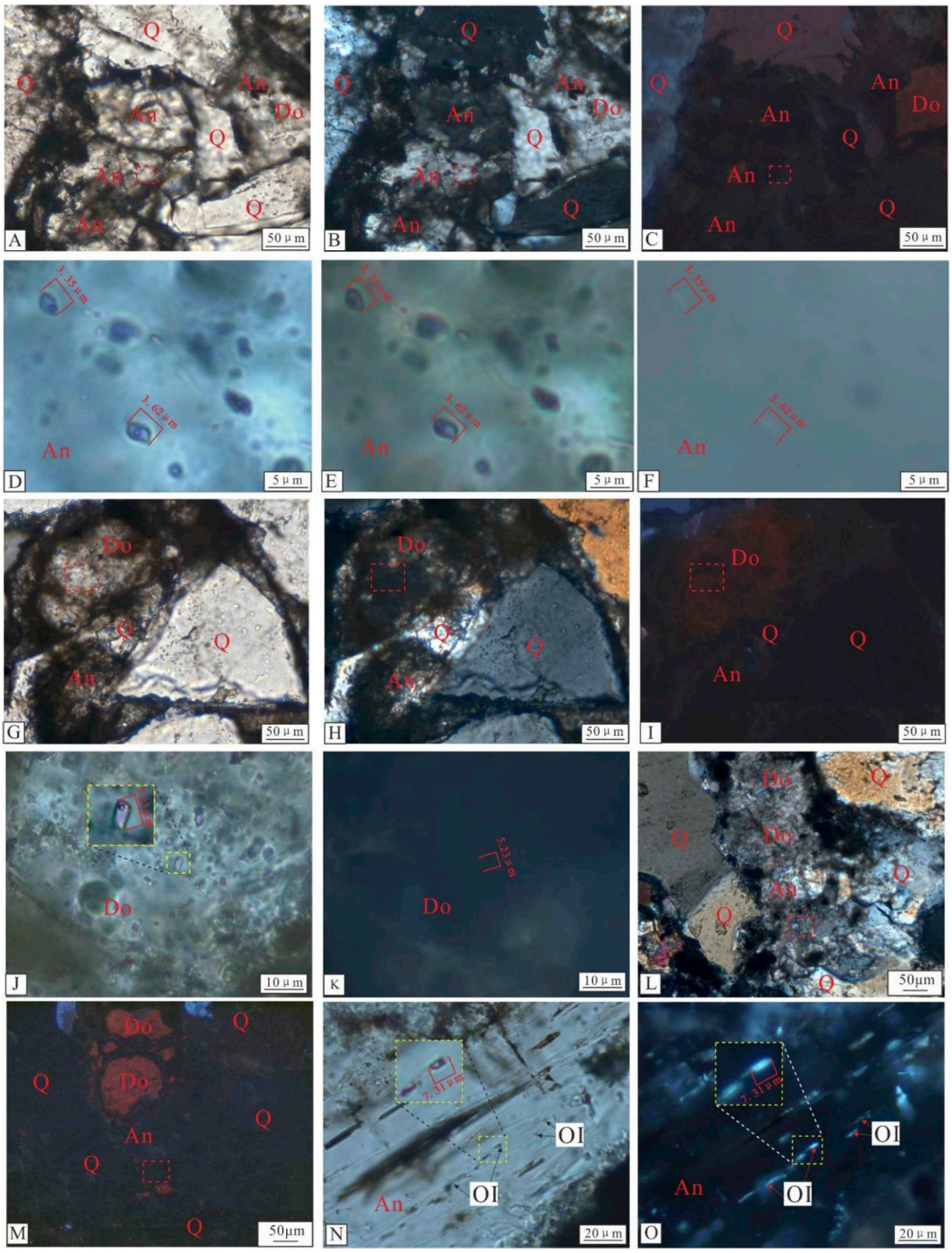

Plate 4. Photomicrographs of oil inclusions and aqueous inclusions trapped in dolomite and ankerite cement in the Es4s reservoirs in the Yanxie229 area. (A) Well Y229-x2, 3755.85 m, ankerite cement, under plane-polarized light, (B) the same field view as (A), under cross-polarized light; (C) the same field view as (A), under cathodoluminescence. Ankerite does not emit luminescence under CL. (D), (E) and (F) were the enlargement of the red dash rectangle in (A). (D), (E) and (F) were taken under plane-polarized light, cross-polarized light and ultraviolet light; the two-phase aqueous inclusions in ankerite cement do not emit fluorescence under ultraviolet light. (G) Well Y229-x2, 3755.85 m, dolomite cement, under plane-polarized light, (H) the same field view as (G), under cross-polarized light; (I) the same field view as (G), under cathodoluminescence. Dolomite cement emit dark red luminescence under CL. (J) and (K) were the enlargement of the red dash rectangle in (G). (J) and (K) were taken under plane-polarized light, and ultraviolet light; the two-phase aqueous inclusions in dolomite cement do not emit fluorescence under ultraviolet light. (L) Well Y229-x2, 3755.85 m, dolomite and ankerite cement under cross-polarized light. (M) the same field view as (L), under cathodoluminescence. Ankerite does not emit luminescence under CL. Dolomite cement emits dark red luminescence under CL. (N) and (O) were the enlargement of the red dash rectangle in (L). (N) and (O) were taken under plane-polarized light, and ultraviolet light; the two-phase oil inclusions in ankerite cements emit yellow fluorescence under ultraviolet light.

Appendix B. Supplementary data

Supplementary data to this article can be found online at https://doi.org/10.1016/j.marpetgeo.2019.104063.

References

Aase, N.E., Walderhaug, O., 2005. The effect of hydrocarbons on quartz cementation: diagenesis in the upper Jurassic sandstones of the miller field, North Sea, revisited. Pet. Geosci. 11 (3), 215–223.

Barclay, S.A., Worden, R.H., 2000. Effects of reservoir wettability on quartz cementation in oil fields. Spec. Publ. Int.: Ass. Sediment 29, 103–117.

Bian, F.Q., 2009. The Restored Eroded Thickness and Prototype Basin of Kongdian Formation and the Fourth Member of the Shahejie Formation in Dongying Depression, vol. 2009. Ocean University of China. College of Marine Geosciences, Qingdao, pp. 20–33.

Bjørkum, P.A., Walderhaug, O., 1993. Isotopic composition of a calcite-cemented layer in the Lower Jurassic Bridport Sands, southern England: implications for formation of laterally extensive calcite-cemented layers. J. Sediment. Petrol. 63 (4), 678–682.

Bjørlykke, K., Jahren, J., 2012. Open or closed geochemical systems during diagenesis in sedimentary basins: constraints on mass transfer during diagenesis and the prediction of porosity in sandstone and carbonate reservoirs. AAPG (Am. Assoc. Pet. Geol.) Bull. 96 (12), 2193–2214.

Bloch, S., Lander, R.H., Bonnell, L., 2002. Anomalously high porosity and permeability in deeply buried sandstone reservoirs: origin and predictability. AAPG (Am. Assoc. Pet. Geol.) Bull. 86 (2), 301–328.

Bourdet, J., Eadington, P., Volk, H., George, S.C., Pironon, J., Kempton, R., 2012. Chemical changes of fluid inclusion oil trapped during the evolution of an oil reservoir: jabiru-1A case study (Timor Sea, Australia). Mar. Pet. Geol. 36 (1), 118–139.

Bukar, M., 2013. Does oil emplacement stop diagenesis and quartz cementation in deeply buried sandstone reservoirs: university of liverpool, department of earth, ocean and ecological sciences. 36, 54 2013.

Cai, C.F., Gu, J.Y., Cai, H.M., 2001. Effect of hydrocarbon emplacement on diagenesis of silurian sandstone of central tarim basin. Acta Sedimentol. Sin. 19 (1), 60–65.

Cao, Y., Yuan, G., Li, X., Wang, Y., Xi, K., Wang, X., Jia, Zh, 2014. Characteristics and origin of abnormally high porosity zones in buried paleogene clastic reservoirs in the shengtuo area, dongying sag, east China. Pet. Sci. 11 (3), 346–362.

Cao, J., Hu, W.X., Xie, X.M., Wang, X.L., Yao, S.P., 2007. Integrate GOI and composition data of oil inclusions to reconstruct petroleum charge history of gas-condensate reservoirs: example from the Mosuowan area, central Junggar basin (NW China). Acta Petrologica Sinica 23 (1), 137–144.

Cao, Y.C., Ma, B.B., Kenneth, E., Jia, Y.C., Wang, Y.Z., 2016. Fluid flow and related diagenetic processes in a rift basin: evidence from the fourth member of the Eocene Shahejie Formation interval, Dongying depression, Bohai Bay Basin, China. AAPG (Am. Assoc. Pet. Geol.) Bull. 100 (11), 1633–1662.

Cao, Y., Wang, Y., Gluyas, J.G., Liu, H., Liu, H., Song, M., 2018. Depositional model for lacustrine nearshore subaqueous fans in a rift basin: the eocene shahejie formation, dongying sag, bohai bay basin, China. Sedimentology 65 (6), 2117–2148.

Chen, Y., Ge, Y.J., Zhou, Z.Z., Mao, C., 2011. Experimental study of the constraint of minerals wettability on hydrocarbon-bearing inclusions forming in reservoir. Acta Geol. Sin. 85 (4), 569–575.

Cox, P.A., Wood, R.A., Dickson, J.A.D., Rougha, H.B.A., Shebl, H., Corbett, P.W.M., 2010. Dynamics of cementation in response to oil charge: evidence from a cretaceous carbonate field. UAE: Sediment. Geol. 228 (3), 246–254.

Dixon, S.A., Summers, D.M., Surdam, R.C., 1989. Diagenesis and preservation of porosity in norphlet formation (upper jurassic), southern Alabama. AAPG (Am. Assoc. Pet. Geol.) Bull. 73 (6), 707–728.

Dutton, S.P., Loucks, R.G., 2010. Reprint of: Diagenetic controls on evolution of porosity and permeability in lower Tertiary Wilcox sandstones from shallow to ultradeep (200–6700 m) burial, Gulf of Mexico Basin, U.S.A. Mar. Pet. Geol. 27 (8), 1775–1787.

Eadington, P.J., Lisk, M., Krieger, F.W., 1996. Identifying Oil Well Sites. US, US 5543616 A.

Ehrenberg, S.N., 1990. Relationship between diagenesis and reservoir quality in sandstones of the Garn Formation, Haltenbanken, Mid-Norwegian Continental Shelf. AAPG (Am. Assoc. Pet. Geol.) Bull. 74 (10), 1538–1558.

Ehrenberg, S.N., Morad, S., Liu, Y.X., Chen, R.L., 2016. Stylolites and porosity in a lower cretaceous limestone reservoir, Onshore Abu Dhabi, U.A.E. J. Sediment. Res. 86 (10), 1228–1247 (2016).

Folk, R.L., Andrews, P.B., Lewis, D., 1970. Detrital sedimentary rock classification and nomenclature for use in New Zealand. N. Z. J. Geol. Geophys. 13 (4), 937–968.

Friedman, I., O'Neil, J.R., 1977. Compilation of stable isotope fractionation factors of geochemical interest. US Government Printing Office.

Friis, H., Molenaar, N., Thomas, Varming, 2014. Chlorite meniscus cement – implications for diagenetic mineral growth after oil emplacement. Terra. Nova 26 (1), 14–21.

Gaupp, R.A., Matter, K., Ramseyer, Platt, J., Walzebuck, J., 1993. Diagenesis and Fluid Evolution of Deeply Buried Permian (Rotliegende) Gas-Reservoirs, Northwest Germany. AAPG (Am. Assoc. Pet. Geol.) Bull. 77 (7), 1111–1128.

George, S.C., Ahmed, M., Liu, K.Y., Volk, H., 2004. The analysis of oil trapped during secondary migration. Organic Geochemistry 35 (11–12), 1489–1511.

George, S.C., Ruble, T.E., Dutkiew icz, A., Eadington, P.J., 2001. Assessing the maturity of oil trapped in fluid inclusions using molecular geochemistry data and visually-determined fluorescence colors. Appl. Geochem. 16 (4), 451–473.

Giles, M.R., Stevenson, S.V., Martin, S.J., Cannon, S.J.C., Hamilton, P.J., Marshall, J.D., Samways, G.M., 1992. The reservoir properties and diagenesis of the Brent Group: A regional perspective: Geology of the Brent Group. Geol. Soc., Lond., Spec. Publ. 61 (1), 289–327.

Gluyas, J.G., Robinson, A.G., Emery, D., Grant, S.M., Oxtoby, N.H., 1993. The link between petroleum emplacement and sandstone cementation In Petroleum Geology of NW Europe. Pet.Geol. Conf. Series 4 (1), 1395–1402.

Goldstein, R.H., 2001. Fluid inclusions in sedimentary and diagenetic systems. Lithos 55 (1–4), 159–193.

Goldstein, R.H., 2003. Petrographic analysis of fluid inclusions. In: In: Samsom, I., Anderson, Marshall, D. (Eds.), Fluid Inclusions – Analysis and Interpretation. Mineralogical Association of Canada, Short Course Series, vol. 32. pp. 9–53.

Goldstein, R.H., Reynolds, T.J., 1994. Systematics of Fluid Inclusions in Diagenetic Minerals, vol. 31 Sepm Short Course.

Gong, Y.J., Liu, S.B., Zhao, M.J., Jiang, L., Gao, X.H., 2016. A new method of underground oil saturation measurement for tight oil-water layer and a case study. Natural Gas Geosci. 27 (12), 2154–2159.

Guo, X.W., Liu, K.Y., He, S., Song, G.Q., Wang, Y.S., Hao, X.F., Wang, B.J., 2012. Petroleum generation and charge history of the northern Dongying Depression, Bohai Bay Basin, China: Insight from integrated fluid inclusion analysis and basin modelling. Mar. Pet. Geol. 32, 21–35.

Hamilton, P.J., Giles, M.R., Ainsworth, P., 1992. K-Ar dating of illites in Brent Group reservoirs: a regional perspective. Geol. Soc. Lond. Spec. Publ., 61 (1), 377–400.

Haszeldine, R.S., Cavanagh, A.J., England, G.L., 2003. Effects of oil charge on illite dates and stopping quartz cement: calibration of basin models. Journal of Geochemical Exploration 78, 373–376.

Haszeldine, R.S., Samson, I.M., Cornford, C., 1984. Dating diagenesis in a petroleum basin, a new fluid inclusion method. Nature 307 (5949), 354–357.

Hawkins, P.J., 1978. Relationship between diagenesis, porosity reduction, and oil emplacement in late Carboniferous sandstone reservoirs. Bothamshall Oilfield, E Midlands: J. Geol. Soc., Lond. 135 (1), 7–24.

Hielmeland, O.S., Larrondo, L.E., 1986. Experimental Investigation of the Effects of Temperature, Pressure, and Crude Oil Composition on Interfacial Properties. Soc. Pet. Eng. 1 (4), 321–328.

Horita, J., 2014. Oxygen and carbon isotope fractionation in the system dolomite-water-CO2 to elevated temperatures. Geochimica et Cosmochimica Acta 129 (8), 111–124.

JI, Y.L., GAO, C.L., LIU, Y.R., LU, H., 2015. Influence of Hydrocarbon Charging to the Reservoir Property in 1st Member of Funning Formation in Gaoyou Depression. J. Tongji Univ. Nat. Sci. 43 (1), 133–139.

Karlsen, D.A., Nedkvitne, T., Larter, S.R., Bjørlykke, K., 1993. Hydrocarbon composition of authigenic inclusions: application to elucidation of petroleum reservoir filling history. Geochem. Cosmochim. Acta 57 (15), 3641–3659.

Kerkhof, A., Hein, U., 2001. Fluid inclusion petrography. Lithos 55, 27–47.

Kim, S.T., O'Neil, J.R., 1997. Equilibrium and nonequilibrium oxygen isotope effects in synthetic carbonates. Geochimica et cosmochimica acta 61 (16), 3461–3475.

Kolchugin, A.N., Immenhauser, A., Walter, B.F., Morozov, V.P., 2016. Diagenesis of the palaeo-oil-water transition zone in a Lower Pennsylvanian carbonate reservoir: Constraints from cathodoluminescence microscopy, microthermometry, and isotope geochemistry. Mar. Pet. Geol. 72 (1), 45–61.

Lisk, M., O'Brien, G.W., Eadington, P.J., 2002. Quantitative evaluation of the oil-leg potential in the Oliver gas field. Timor Sea, Australia: AAPG (Am. Assoc. Pet. Geol.) Bull. 86 (9), 1531–1542.

Liu, G.B., 1979. Crystal defects and formation mechanism of gas-liquid inclusions: Chinese Science. Bulletin 24 (3), 115–119.

Liu, K.Y., Eadington, P., 2005. Quantitative fluorescence techniques for detecting residual oils and reconstructing hydrocarbon charge history. Org. Geochem. 36 (7), 1023–1036.

Liu, K., Bourdet, J., Zhang, B., Zhang, N., Lu, X.S., Liu, S.B., Pang, H., Zhou, L., Guo, X.W., 2013. Hydrocarbon charge history of the Tazhong Ordovician reservoirs, Tarim basin as revealed from an integrated fluid inclusion study. Pet. Explor. Dev. Online 40 (2), 183–193.

Ma, B.B., Eriksson, K.,A., Cao, Y.C., Jia, Y.C., Wang, Y., Z., Gill, B.C., 2016. Fluid flow and related diagenetic processes in a rift basin: Evidence from the fourth member of the Eocene Shahejie Formation interval, Dongying depression, Bohai Bay Basin, China. AAPG (Am. Assoc. Pet. Geol.) Bull. 100 (11), 1633–1662.

Mansurbeg, H., Morad, S., Salem, A., Marfil, R., El-ghali, M.A.K., Nystuen, J.P., Caja, M.A., Amorosi, A., Garcia, D., La lglesia, A., 2008. Diagenesis and reservoir quality evolution of palaeocene deep-water, marine sandstones, the Shetland-Faroes Basin. British Cont. Shelf: Mar. Pet. Geol. 25 (6), 514–543.

Marchand, A.M.E., Haszeldine, R.S., Macaulay, C.I., Swennen, R., Fallick, A.E., 2000. Quartz cementation inhibited by crestal oil charge: Miller deep water sandstone. UK North Sea: Clay Miner. 35 (1), 205–214.

Marchand, A.M.E., Haszeldine, R.S., Smalley, P.C., Macaulay, C.I., Fallick, A.E., 2001. Evidence for reduced quartz-cementation rates in oil-filled sandstones. Geology 29 (10), 915–918.

Marchand, A.M.E., Smalley, P.C., Haszeldine, R.S., Fallick, A.E., 2002. Note on the importance of hydrocarbon fill for reservoir quality prediction in sandstones. AAPG (Am. Assoc. Pet. Geol.) Bull. 86 (9), 1561–1571.

Mclimans, R.K., 1987. The application of fluid inclusions to migration of oil and diagenesis in petroleum reservoirs. Appl. Geochem. 2 (5), 585–603.

Meng, Y.L., Pan, X.M., Wu, H.Y., Wang, C., Li, M.M., Zhang, A.D., Xiu, H.W., Wang, Z.W., 2010. Porosity and oil saturation correlation and diagenetic retardation of sandstone by hydrocarbon emplacement in the shallow-middle strata of the northern Songliao Basin. Bull. Miner. Petrol. Geochem. 29 (1), 11–16.

Molenaar, N., Cyziene, J., Sliaupa, S., Craven, J., 2008. Lack of inhibiting effect of oil emplacement on quartz cementation: Evidence from Cambrian reservoir sandstones, Paleozoic Baltic Basin. Geol. Soc. Am. Bull. 120 (9), 1280–1295.

Morad, A., Winters, B., Stevens, R., White, E., Weingart, J., Yaster, M., Gottschalk, A., 2012. The efficacy of intravenous patient-controlled analgesia after intracranial surgery of the posterior fossa: a prospective, randomized controlled trial. Anesth. Analg. 114 (2), 416–423.

Munz, I.A., 2001. Petroleum inclusions in sedimentary basins: systematics, analytical

methods and applications. Lithos 55 (1), 195–212.
Nedkvitne, T., Karlsen, D.A., Bjørlykke, K., Larter, S.R., 1993. Relationship between reservoir diagenetic evolution and petroleum emplacement in the Ula Field. North Sea: Mar. Pet. Geol. 10 (3), 255–270.
Neilson, J.E., Oxtoby, N.H., Simmons, M.D., Simpson, I.R., Fortunatova, N.K., 1998. The relationship between petroleum emplacement and carbonate reservoir quality: examples from Abu Dhabi and the Amu Darya Basin. Mar. Pet. Geol. 15 (1), 57–72.
Neveux, L., Grgic, D., Carpentier, C., Pironon, J., Girard, J.P., 2014. Influence of hydrocarbon injection on the compaction by pressure solution of a carbonate rock: An experimental study under triaxial stresses. Mar. Pet. Geol. 55 (8), 282–294.
Oxtoby, N.H., Mitchell, A.W., Gluyas, J.G., 1995. In: Cubitt, J.M., England, W.A. (Eds.), The Filling and Emptying of the Ula Oilfield (Norwegian North Sea), Geol Soc. Sec. Publ.No. 86, the Geochemistry of Reservoirs, pp. 141–158.
Paganni, M.M., Harthi, A.A., Morad, D., Morad, S., Ceriani, A., 2016. Impact of stylolitization on diagenesis of a Lower Cretaceous carbonate reservoir from a giant oilfield, Abu Dhabi. United Arab Emirates: Sediment. Geol. 335 (15), 70–92.
Paganoni, M., Al Harethi, A., Morad, D., Morad, S., Ceriani, A., Mansurbeg, H., Al Suwaidi, A., Al-Aasm, I.S., Ehrenberg, S.N., Sirat, M., Dhabi, A., 2015. Impact of stylolitization on diagenesis and reservoir quality: A case study from an Early Cretaceous reservoir in a Giant oilfield, Abu Dhabi, United Arba Emirates. Soc. Pet. Eng. Int. 1–20 SPE-177944-MS.
Parnell, J., Middleton, D., Honghan, C., Hall, D., 2001. The use of integrated fluid inclusion studies in constraining oil charge history and reservoir compartmentation: examples from the Jeanne d'Arc Basin, offshore Newfoundland. Mar. Pet. Geol. 18 (5), 535–549.
Ping, H., Chen, H., Thiéry, R., George, S.C., 2017. Effects of oil cracking on fluorescence color, homogenization temperature and trapping pressure reconstruction of oil inclusions from deeply buried reservoirs in the northern dongying depression, Bohai bay basin, china. Mar. Pet. Geol. 80 (2), 538–562.
Prieto, M., Paniagua, A., Marcos, C., 1996. Formation of primary fluid inclusions under influence of the hydrodynamic environment. Eur. J. Mineral. 8 (5), 987–996.
Prozorovich, G.E., 1970. Determination of the time of oil and gas accumulation by epigenic studies. Sedimentology 15 (1–2), 41–52.
Qi, Y.K., Luo, X.R., Wang, Y., Liu, N.G., Zhou, B., Yan, J.Z., Zhang, L.K., 2017. Mechanical study of the effect of fractional-wettability on multiphase fluid flow. Int. J. Multiph. Flow 93, 205–212.
Qiu, N.S., Su, X.G., Li, Z.Y., Liu, Z.Q., Li, Z., 2006. The Cenozoic tectono-thermal evolution of Jiyang depression, Bohai bay basin, East China. Chin. J. Geophys. 49 (04), 1127–1135.
Ramm, M., Bjørlykke, K., 1994. Porosity/depth trends in reservoir sandstones: Assessing the quantitative effects of varying pore-pressure, temperature history and mineralogy, Norwegian Shelf data. Clay Miner. 29 (4), 475–490.
Robin, M., Rosenberg, E., Fassi-Fihri, O., 1995. Wettability studies at the pore level: a new approach by use of Cryo-SEM. SPE Form. Eval. 10 (1), 11–19.
Saigal, G.C., Bjørlykke, K., Larter, S., 1992. The effects of oil emplacement in diagenetic processes-Examples from the Fulmar reservoir sandstones: Central North Sea. AAPG (Am. Assoc. Pet. Geol.) Bull. 76 (7), 1024–1033.
Sathar, S., Worden, R.H., Faulkner, D.R., Smalley, P.C., 2012. The effect of oil Saturation on the mechanism of compaction in granular materials: Higher oil saturations lead to more grain fracturing and less pressure solution. J. Sediment. Res. 82 (7–8), 571–584.
Stasiuk, L.D., Snowdon, L.R., 1997. Fluorescence micro-spectrometry of synthetic and natural hydrocarbon fluid inclusions: crude oil chemistry, density and application to petroleum migration. Appl. Geochem. 12 (3), 229–241.
Su, A., Chen, H.H., Ping, H.W., 2015. Secondary alterations influence on fluorescence color and spectral parameters of crude oil and oil inclusion. Spectrosc. Spectr. Anal. 35 (3), 668–673.
Taylor, T.R., Giles, M.R., Hathon, L.A., Diggs, T.N., Braunsdorf, N.R., Birbiglia, G.V., Kittridge, M.G., Macaulay, C.I., Espejo, I.S., 2010. Sandstone diagenesis and reservoir quality prediction: models, myths, and reality. AAPG (Am. Assoc. Pet. Geol.) Bull. 94 (8), 1093–1132.
Tingate, P.R., Rezaee, M.R., 1997. Origin of quartz cement in tirrawarra sandstone, southern cooper basin, South Australia. J. Sediment. Res. 67 (1), 168–177.
Tobin, R.C., McClain, T., Lieber, R.B., Ozkan, A., Banfield, L.A., Marchand, A.M., McRae, L.E., 2010. Reservoir quality modeling of tight-gas sands in Wamsutter field: Integration of diagenesis, petroleum systems, and production data. AAPG Bulletin 94 (8), 1229–1266.
Toledo, P.G., Araujo, Y.C., Leon, V., 1996. Wettability of Oil-Producing Reservoir Rocks as Determined from X-ray Photoelectron Spectroscopy. J. Colloid Interface 183 (2), 301–308.
Walderhaug, O., 1990. A fluid inclusion study of quartz-cemented sandstones from offshore mid-norway–possible evidence for continued quartz cementation during oil emplacement. J. Sediment. Res. 60 (2), 203–210.
Walderhaug, O., 1994. Precipitation rates for quartz cement in sandstones determined by fluid-inclusion microthermometry and temperature-history modeling. J. Sediment. Res. 64 (2), 324–333.
Wang, Q., Shi, J.A., Xiao, L.X., Xue, L.H., 1998. Influence of Oil Emplacement on Diagenetic Sequence of the Clastic Reservoir Rock and It's Relationship to the Porosity Evolution ——Taking the Carboniferous quartz sandstone in southeast Tarim depression as an example. Acta Sedimentol. Sin. 16 (3), 97–101.
Wang, F.Y., Pang, X.Q., Zeng, J.H., Shi, Y.L., Hu, J.F., 2005. Paleo-Oil Leg Recognition and Its Application to Petroleum Exploration. Xinjing Pet. Geol. 26 (5), 565–569.
Wang, Y.Z., Cao, Y.C., Ma, B.B., 2014. Mechanism of diagenetic trap formation in nearshore subaqueous fans on steep rift lacustrine basin slopes—a case study from the Shahejie Formation on the north slope of the Minfeng Subsag, Bohai Basin, China. Pet. Sci. 11 (4), 481–494.
Wang, Y.Z., Cao, Y.C., Zhang, S.M., Li, F.L., Meng, F.C., 2016. Genetic mechanisms of secondary pore development zones of Es4x. In: The North Zone of the Minfeng Sag in the Dongying Depression, East China: Petroleum Science, vol. 13. pp. 1–17 (1).
Wang, Y., Lin, M., Xi, K., Cao, Y., Wang, J., Yuan, G., Song, M.S., 2018. Characteristics and origin of the major authigenic minerals and their impacts on reservoir quality in the Permian Wutonggou formation of Fukang sag, Junggar basin, western china. Mar. Pet. Geol. 97 (9), 241–259.
Worden, R.H., Morad, S., 2000. Quartz cementation inoil field sandstones: a review of the key controversies. In: In: Worden, R.H., Morad, S. (Eds.), Quartz Cementation in Sandstones, vol. 29. International Association of Sedimentologists Special Publication, pp. 1–20.
Worden, R.H., Morad, S., 2003. Clay Minerals in Sandstones: Controls on Formation. Distribution and Evolution.
Worden, R.H., Oxtoby, N.H., Smalley, P.C., 1998. Can oil emplacement prevent quartz cementation in sandstones? Pet. Geosci. 4 (2), 129–137.
Worden, R.H., Bukar, M., Shell, P., 2018. The effect of oil emplacement on quartz cementation in a deeply buried sandstone reservoir. AAPG (Am. Assoc. Pet. Geol.) Bull. 102 (1), 49–75.
Wu, Z., Han, W.G., 2000. Erosiveness under the hiatus between Paleogene and Neogene in depression. China Offshore Oil Gas Geol. 14 (5), 320–323.
Xi, K.L., Cao, Y.C., Wang, Y.Z., Zhang, Q.Q., Jin, J.H., Zhu, R.K., Zhang, S.M., Wang, J., Yang, T., Du, L.H., 2015a. Factors influencing physical property evolution in sandstone mechanical compaction: the evidence from diagenetic simulation experiments. Pet. Sci. 12 (3), 391–405.
Xi, K., Cao, Y., Jahren, J., Zhu, R., Bjørlykke, K., Zhang, X., Cai, L., Hellevang, H., 2015b. Quartz cement and its origin in tight sandstone reservoirs of the Cretaceous Quantou formation in the southern Songliao basin, China. Mar. Pet. Geol. 66 (4), 748–763.
Xie, X.M., Cao, J., Hu, W.X., Zhang, Y. j, Wang, X.L., Zhang, Y.Q., Tang, Y., 2007. Origin and Application of GOI Data of Oil Inclusions in Structurally ComplexBasins :A Case Study in the Mosuowan Area of the Junggar Basin (NW China). Acta Geological Sinica 81 (6), 834–842.
Yan, J.Z., Luo, X.R., Zhang, L.K., Lei, Y.H., 2012. Experimental study on percolation backbone of secondary migration of crude oil. Pet. Geol. Exp. 34 (1), 99–103.
Yang, T., Cao, Y., Friis, H., Liu, K.Y., Wang, Y.Z., Zhou, L.L., Zhang, S.M., Zhang, H.N., et al., 2017. Genesis and distribution pattern of carbonate cements in lacustrine deep-water gravity-flow sandstone reservoirs in the third member of the Shahejie Formation in the Dongying Sag, Jiyang Depression, Eastern China. Mar. Pet. Geol. 90, 547–564.
Yuan, Z., Li, W.H., Guo, Y.Q., 2011. Effects of oil emplacement on diagenetic evolution of sandstone reservoir in Yanchang Formation, Southeastern Ordos Basin. Geol. J. China Univ. 17 (4), 594–604.
Yuan, G., Cao, Y., Gluyas, J., Li, X.Y., Xi, K.L., Wang, Y.Z., Jia, Z.Z., Sun, P.P., Norman, H. Oxtoby, 2015. Feldspar dissolution, authigenic clays, and quartz cements in open and closed sandstone geochemical systems during diagenesis: Typical examples from two sags in Bohai Bay Basin, East China. AAPG (Am. Assoc. Pet. Geol.) Bull. 99 (11), 2121–2154.
Yuan, G., Cao, Y., Gluyas, J., Cao, X., Zhang, W.B., 2018. Petrography, fluid inclusion, isotope and trace element constraints on the origin of quartz cementation and feldspar dissolution and the associated fluid evolution in arkosic sandstones. AAPG (Am. Assoc. Pet. Geol.) Bull. 102 (5), 761–792.
Yuan, G., Cao, Y.C., Zan, N.M., Schulz, H.M., Gluyas, J., Hao, F., Jin, Q., Liu, K.Y., Wang, Y.Z., Chen, Z.H., Jia, Z.Z., 2019. Coupled mineral alteration and oil degradation in thermal oil-water-feldspar systems and implications for organic-inorganic interactions in hydrocarbon reservoirs. Geochem. Cosmochim. Acta 248 (1), 61–87.
Zhang, P., Tweheyo, M.T., Austad, T., 2007. Wettability alteration and improved oil recovery by spontaneous imbibition of seawater into chalk: Impact of the potential determining ions Ca^{2+}, Mg^{2+}, and SO_4^{2-}. Colloid. Surf. Physicochem. Eng. Asp. 301 (1), 199–208.
Zhang, Q., Zhu, X.M., Steel, R.J., Zhong, D.K., 2014. Variation and mechanisms of clastic reservoir quality in the palaeogene Shahejie Formation of the Dongying sag, Bohai Bay Basin, China. Pet. Sci. 11 (2), 200–210.